MICRO AND NANOSTRUCTURED DEVICES FOR THERMAL ANALYSIS

A THESIS
SUBMITTED TO THE PROGRAM OF MATERIALS SCIENCE AND NANOTECHNOLOGY
AND THE INSTITUTE OF ENGINEERING AND SCIENCES
OF BILKENT UNIVERSITY
IN PARTIAL FULLFILMENT OF THE REQUIREMENTS
FOR THE DEGREE OF
MASTER OF SCIENCE

By
Özlem Şenlik
September, 2008

I certify that I have read this thesis and that in my opinion it is fully adequate, in scope and in quality, as a thesis for the degree of Master of Science.

Assist. Prof. Dr. Mehmet Bayındır (Supervisor)

I certify that I have read this thesis and that in my opinion it is fully adequate, in scope and in quality, as a thesis for the degree of Master of Science.

Ress. Assist. Prof. Dr. Aykutlu Dâna (Co-supervisor)

I certify that I have read this thesis and that in my opinion it is fully adequate, in scope and in quality, as a thesis for the degree of Master of Science.

Prof. Dr. Salim Çıracı

I certify that I have read this thesis and that in my opinion it is fully adequate, in scope and in quality, as a thesis for the degree of Master of Science.

Assist. Prof. Dr. M. Özgür Oktel

I certify that I have read this thesis and that in my opinion it is fully adequate, in scope and in quality, as a thesis for the degree of Master of Science.

_____

Assist. Prof. Dr. Ali Kemal Okyay

Approved for the Institute of Engineering and Sciences:

_____

Prof. Dr. Mehmet B. Baray

Director of Institute of Engineering and Sciences

ABSTRACT
MICRO AND NANOSTRUCTURED DEVICES FOR THERMAL ANALYSIS

Özlem Şenlik

M.S. in Graduate Program of Materials Science and Nanotechnology

Supervisor: Assist. Prof. Dr. Mehmet Bayındır

September 2008

The recent advent of micro and nano devices increased the interest in small scale material properties, such as elasticity, conductivity or heat capacity, which are considerably different from their bulk counterparts due to, primarily, increasing surface to volume ratios. These novel properties must be analyzed by using ultra-sensitive devices since characterization of these properties is not possible with conventional probing instrumentation due to their large mass or volume which decreases signal to noise ratio. Microelectromechanical systems (MEMS) with short response time and high sensitivity are suitable for such measurements, such as very small mass detection (zeptograms) and calorimetry of small volume materials (yoctocalories).

In this thesis a MEMS cantilever was used for thermomechanical characterization of thin film amorphous semiconductors. 100 nm thick As_2S_3 and Ge-As-Se-Te glasses were thermally evaporated onto a bilayer microcantilever. The microcantilever was deflected and vibrated by electrothermal actuation. By monitoring deflection, amplitude and phase of the cantilever oscillation, multiple glass transition and melting points were identified; the effects of the variation of thermal expansion coefficients (CTE), reversible and irreversible heat capacities and Young's modulus of the thin film samples were observed simultaneously. Hence the possibility of the integration

of calorimetry, thermomechanical analysis (TMA) and dynamical mechanical thermal analysis (DMTA) in a single MEMS device was demonstrate

Keywords: Nanocalorimetry, Thermal Methods, MEMS/NEMS, Electro-Thermal Actuation, Thin Films

ÖZET

TERMAL ANALİZLER İÇİN MİKRO VE NANO YAPILI AYGITLAR

Özlem Şenlik

Malzeme Bilimi ve Nanoteknolji Yüksek Lisans Programı Yüksek Lisans

Tez Yöneticisi: Yar. Doç. Prof. Dr. Mehmet Bayındır

Eylül 2008

Yakın zamanda mikro ve nano aygıtların yaygınlaşması, küçük ölçekli malzemelerin elastisite, iletkenlik, ısı sığası gibi, yığın malzemelerinkinden tamamen farklı özelliklerine olan ilgiyi arttırdı. Bu yeni özelliklerin çok hassas aygıtlar ile karakterize edilmesi gerekmektedir. Mikroelektromekanik sistemler (MEMS) kısa zaman tepkisi ve yüksek hassasiyeti ile bu tür malzemelerin özelliklerinin belirlenmesi için uygundur.

Bu tezde, ince film, amorf yarı iletkenlerin termomekanik karakterizaasyonu bir MEMS manivela kullanılarak ölçülmüştür. 100 nm kalınlığında AS_2S_3 ve Ge-As-Se-Te camsı malzemeler buharlaştırma yöntemi ile manivela üzerine kaplanmıştır. Manivela elektrotermal tahrik ile bükülmüş ve titreştirilmiştir. Manivelanın bükülmesi, titreşiminin genliği ve fazı ölçülerek çoklu camsı geçiş ve erime noktası tayin edilmiş; ince film örneklerin ısısal genleşme katsayısının değişiminin etkisi, tersinir ve tersinmez ısı sığaları ve Young miyarları izlenmiştir. Böylece kalorimetre termomekanik analiz ve dinamik mekanik termal analiz yöntemleri tek bir MEMS aygıtında birleştirilmiştir.

Anahtar Kelimeler: Nanokalorimetre, Termal Yöntemler, MEMS/ NEMS, Elektro-Termal Tahrik, İnce Film

Acknowledgements

First of all, I would like to express my indebtedness to my supervisors Prof. Mehmet Bayındır and Prof. Aykutlu Dana for their encouragement and guidance. I would like to thank Prof. Aykutlu Dana once more for introducing me microsystems and teaching his experience during long hours spent in laboratory.

I would also like to thank Prof. Dr. Salim Çıracı for his valuable effort in the establishment of Nanotechnology Research Center (UNAM), Bilkent and Advanced Research Laboratory (İAL), Bilkent of which I used laboratory facilities.

I greatly appreciate my group members: Hasan Güner, Ozan Aktaş, M. Kurtuluş Abak, Dr. Mecit Yaman, and H. Esat Kondakçı and UNAM engineers: A. Koray Mızrak and Burkan Kaplan for their valuable help for fabrication and measurement steps. Also, thanks to Tarık Çeber for his immediate functional solutions in technical issues.

I greatly enjoyed working with Bayındır Group members: Dr. Abdullah Tülek, Kemal Gürel, C. Murat Kılınç, Mert Vural, Duygu Akbulut, Yavuz N. Ertaş, Özlem Köylü, Adem Yıldırım, Hülya Budunoğlu and Sencer Ayas. Their sincere friendship formed an elegant working atmosphere.

I wish to give my special thanks to my parents, my sister Ülkü and my husband Servet Seçkin. This thesis would be impossible without their support, encouragement and love. I especially appreciate Servet's patience during writing of this thesis.

The financial support from TUBİTAK and Republic of Turkey Health Ministry is also gratefully acknowledged.

Table of Contents

List of Figures

List of Tables

Chapter 1

Introduction

Determination of material properties is essential for all technological applications. Physical properties of materials vary with environmental factors such as temperature, pressure, or humidity. Among these factors thermal effects arouse special interest. Temperature increases induce first order thermal transitions, such as melting and evaporation, and/or second order phase transitions, such as glass transition. These thermal transitions give rise to variation in diverse material properties such as heat capacity, Young modulus, thermal expansion coefficient, and mechanical loss. The observation of material behavior and quantitative measurement of these physical changes can yield ample information on the nature of a physical or chemical process involved. So far, many thermal characterization methods have been developed in order to characterize thermal properties of materials; calorimetry, thermomechanical analysis, and dynamic mechanical thermal analysis are among the most popular thermal analysis methods.

Until recently, thermal instrumentation methods only provide the opportunity to characterize properties of only bulk material because of sensitivity limitations. With the advent of nanotechnology, small scale materials of current scientific and technological interest can be made in thin film form or using nano scale particles. Examples of such materials include multilayers, many amorphous materials, ultrathin films of reduced size, and nanocrystals. This reduction in dimension usually has remarkable effect on thermodynamic properties. Thin film properties are considerably different than that of the same material in bulk form because surface and interfacial effects become dominant at small scales where the total fraction of atoms at the surface is significant. The big difference between bulk properties and small volume materials reveals the need for new

characterization tools. Determination of thermal and mechanical properties of small volume materials can be possible by using ultra-sensitive micro/nano structured devices.

Recently microelectromechanical (MEMS) sensors with compact sizes combined with very high sensitivities and short response times have been introduced. For example, the sensitivity of a *bimetallic microelectromechanical sensor* is on the order of picojoules, and typical time responses are microseconds. Therefore MEMS sensors are very promising in fields where the sample quantity to be measured is less than a nanogram, *e.g.* in biochemistry or surface science. Moreover, fast time resolution of MEMS devices expands the power to investigate dynamic processes in chemical reactions and thermal transitions.

The thermal analysis sensor presented in this thesis is a bimetallic microthermoelectromechanical lever. The sample investigated, can be spin coated or deposited by physical vapor deposition (PVD) on the thermal cantilever probe. A small alternating signal imposed on a DC voltage is applied between the two terminals of the cantilever device. In this way the sample is heated via *joule heating*. This kind of heating induces an additional oscillatory temperature on the linearly increasing sample temperature. The temperature rise makes the cantilever deflect and vibrate with the frequency of the AC voltage. Monitoring DC deflection simultaneously with the magnitude and phase of the oscillation, and the analysis of these data enables qualitative and quantitative information about the underlying processes and material properties, *i.e.* thermal transition temperatures, heat capacity, thermal expansion coefficient, Young modulus and viscosity variations associated with these transitions. Therefore, the sensor integrates calorimetry, thermomechanical analysis, and dynamic mechanical thermal analysis in a novel micro machine.

Organization of the thesis is as follows. In Chapter 2, working principles of thermal analysis methods will be explained and recent advances in calorimetry and thermal analysis of small scale materials will be mentioned briefly. In

Chapter 3, analytical calculations are presented for thermomechanical behavior of the multilayer cantilever. In Chapter 4, fabrication process of the sensor, measurement setup is described. Results are discussed critically. Finally, the thesis is concluded with evaluation of the thesis and suggestion of future work

Chapter 2

Theoretical Background

Many properties of the physical world depend on temperature. The temperature of a system is defined as the average kinetic energy of its atoms or molecules. Temperature generally alters with supplement or removal of energy which is the heat exchanged between the system and its enviroment. On the other hand, if sufficient heat is available, instead of further increasing the temperature the system will transform into a more stable state. This transformation may be physical such as glass transition, crystallization, melting, vaporization or it may be chemical which alters the chemical structure of the material. Even biological processes such as metabolism or decomposition may be included. In general these transformations alter material properties, *e.g.* thermal expansion coefficient, heat capacity, enthalpy, entropy, morphology, molecular properties, electrical properties, elastic modulus [1]. Therefore, it is essential that the temperature dependencies of these properties of a material are determined in order to anticipate device performance or process dynamics based on the material.

In order to characterize temperature dependent material properties, various calorimetric and thermal analysis methods have been developed since late 18^{th} century [2]. While *calorimetry* is the general name for the measurement of heat; *thermal analysis* is "a group of techniques in which a property of the sample is monitored against time or temperature while the temperature of the sample, in a specific atmosphere, is programmed" [3]. In Table 2.1, the most frequently used thermal analysis techniques are given together with the quantity measured and the property under study. Specific thermal analysis techniques are sensitive to only some thermal transitions that occur in a material when heated or cooled with a certain heating/ cooling rate. This is due to the fact that different material

properties measured against temperature, by the specific technique, exhibit different variations in the thermal transition range investigated. For example, dynamical mechanical thermal analysis technique (DMTA) can be particularly sensitive to low energy transitions which are not readily observed by calorimetric techniques [4].

Technique	*Abbreviation*	*Propertymeasured*	*Property under study*
Differential Scanning Calorimetry*	DSC	Power Difference Heat Flow	Heat Capacity Phase Changes Reactions
Differential Thermal Analysis	DTA	Temperature Difference	Phase Changes Reactions
Thermomechanical Analysis*	TMA	Deformations	Mechanical Changes Phase Changes
Dynamic Mechanical Thermal Analysis*	DMTA	Dimensional Change Moduli	Expansion Phase Changes Glass Transitions
Dielectric Thermal Analysis	DETA	Electrical	
Thermogravimetry or (Thermogravimetric Analysis)	TG TGA	Mass	Decompositions Oxidations
Thermoptometry		Optical	Phase Changes Surface Reactions Color Changes
Thermosonimetry	TS	Sound	Mechanical and Chemical Changes
Thermoluminescence	TL	Light emitted	Oxidation
Thermomagnetometry	TM	Magnetic	Magnetic Changes, Curie points

Table 2-1Thermal methods. Methods with * are used in the thesis. [4]

Furthermore, many of the thermal transitions are time-dependent necessitating a time resolved measurement with compatible instrumentation setup. This is illustrated for a typical heat flux (ϕ) vs. temperature (T) measurement of a lead sample for heating rates (β) from 5 to 50 K/min in the melting temperature range, *i.e.* 300-400°C. The shifting of the peak temperature (T_p) with respect to heating rate (β) illustrates the time dependency of the thermal transition.

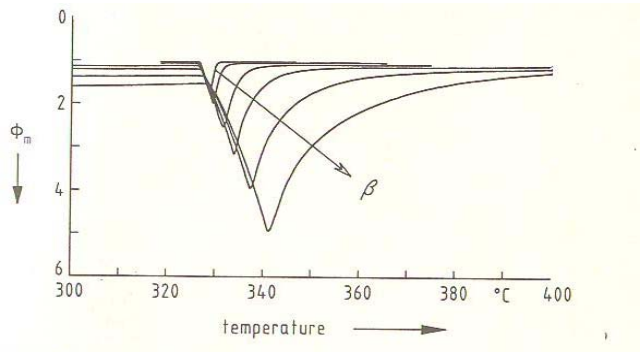

Figure 2-1 Measured curves showing the peak temperature Tp of a melting lead sample changing with heating rate (β) increasing in the arrow direction from 5 to 50 K/min [5].

Materials can be classified according to their morphology as crystalline or amorphous/liquid. For crystalline materials there is a discontinuous decrease in volume at the melting temperature T_m. However, for glassy materials, volume decreases continuously with temperature reduction; a slight decrease in slope of curve occurs at the glass transition temperature T_g (Figure 2-2). Below the glass transition temperature T_g, the material is considered to be a glass; above it is first a supercooled liquid and finally a less viscous liquid.

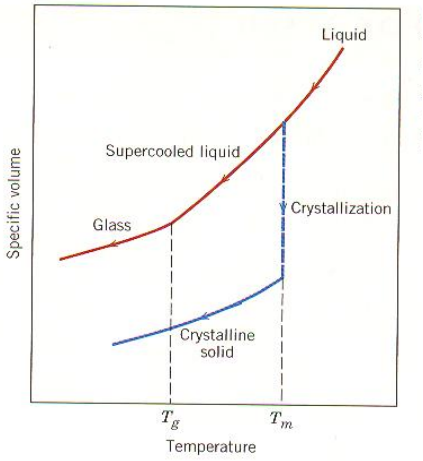

Figure 2-2 Comparison of specific volume vs. temperature behavior of crystalline and amorphous/glassy materials [1].

Specific volume change with temperature is a general characteristic of all materials. This change manifests itself in the alteration of different material properties such as heat capacity, elastic modulus, mechanical loss factor and

thermal expansion coefficient. By monitoring the variation of a set of material properties versus temperature, this critical change in the morphology and related thermal action can be deduced. Even by modulating the applied temperature, dynamical response of the material can be discerned. Calorimetry, thermal mechanical analysis (TMA) and dynamic mechanical thermal analysis (DMTA) are marked in the Table 2.1 with an asterisk. In this thesis, a single thermal analysis device is effectively used to identify mentioned time dependent critical changes, therefore these three methods will be discussed briefly in the next section.

2.1 Calorimetry

Calorimetry is the science of measuring the heat involved in physical or chemical reactions. The heat exchange between a system and its environment either changes the system temperature or induces change on the system. This is described in differential form as

$$dH = U(T) + (dpV + pdV)\,, \tag{2.1}$$

where H is the enthalpy, U is the internal energy, and T is the temperature of the system and $dpV + pdV$ is the work done on or by the system. Monitoring the heat exchange and the induced temperature simultaneously, one can determine associated enthalpies, and the corresponding heat capacity measurements [3-5]. It is useful to classify calorimeters according to the measuring principle, mode of operation, and principle of construction [6].

According to the measuring principle classification the first type is the *heat compensating calorimeters.* These calorimeters compensate the heat to be measured either passively by thermal transition of a calorimeter substance that has well-known thermodynamic properties or by a control system which compensates temperature change through electrical heating/cooling (Joule heating or Peltier cooling [7]). Use of a suitable heat/source sink for compensation is also possible. In this type of calorimeters, the compensated heat energy is determined from the measurement of calorimetric substance

properties, *e.g.* from the mass of the substance that endures thermal transition such as melting or from the electrical heating/cooling energy. The second type, *heat accumulating calorimeters,* measure the temperature change of the calorimeter substance with which the sample is thermally connected. This temperature change is proportional to the amount of heat exchanged between the sample and the calorimeter substance. Finally, in *heat exchanging calorimeters,* a defined heat exchange takes place between the sample and the surroundings (sample container/ support). The heat flow rate is determined on the basis of the temperature difference along a 'thermal resistance' between sample and surroundings. Registration of the time dependence of heat flow rate allows kinetic investigations.

According to their operation modes, in *isothermal calorimeters,* during the measurement, sample and its surrounding are held at a constant temperature. *Isoperibol calorimeters* has a constant temperature jacket that keeps the surrounding at a constant temperature while the sample's temperature may alter during measurement whereas in *adiabatic calorimeters* heat exchange between the sample and its surrounding are prevented by maintaining both of them at the same temperature, which may increase during reaction. For all these operation modes static and dynamic measurement can be performed.

The calorimeters can be constructed either as a *single cell calorimeter* in which sample properties are measured absolutely or as a *twin cell or differential calorimeter* in which measurement is made with respect to a reference.

Calorimeters based on different measurement principles, construction principles and operation modes have distinct advantages, such as sensitivity to heat capacity measurements or latent heat measurements. Obviously not all combinations explained above are feasible. Among many calorimetric measurement types two most frequently used will be emphasized: Differential Scanning Calorimetry and Modulated- Temperature Differential Scanning Calorimetry (MTDSC) [8].

2.1.1 Differential Scanning Calorimetry (DSC)

Differential scanning calorimeters monitor the difference of heat flow rate (ϕ) between the sample and the reference while both of them are exposed to same temperature program

$$T(t) = T_a + \beta t \tag{2.2}$$

where T_a is the ambient temperature, (β) is the heating rate and $T(t)$ is the instantaneous temperature. Alternatively the temperature difference (ΔT) for a defined heat flow rate ($\phi(t)$) can also be monitored [5]. When a sample and a reference is subject to a temperature program as above, while the associated differential heat flow is monitored, thermal transitions that occur in the sample can be observed as shown in Figure 2-3. In Figure 2-3, firstly three thermal transition regions can be identified. The first region is the glass transition which is a second order thermal transition[1]. In this transition region the slope is positive indicating a heat flow rate increase, due to a heat capacity increment. Heat capacity in differential form is

$$C = \frac{\frac{\delta q}{\delta t}}{\frac{\delta T}{\delta t}} = \frac{\delta q}{\delta T}\,, \tag{2.3}$$

where $\frac{\delta q}{\delta t}$ is the heat flow (ϕ). The second thermal transition is crystallization which is a first order thermal transition including latent heat. The shaded area in the crystallization region corresponds to the total amount of latent heat given out by the system. Same reasoning applies to melting which is also a first order transition however in this case latent heat must be supplied to the system.

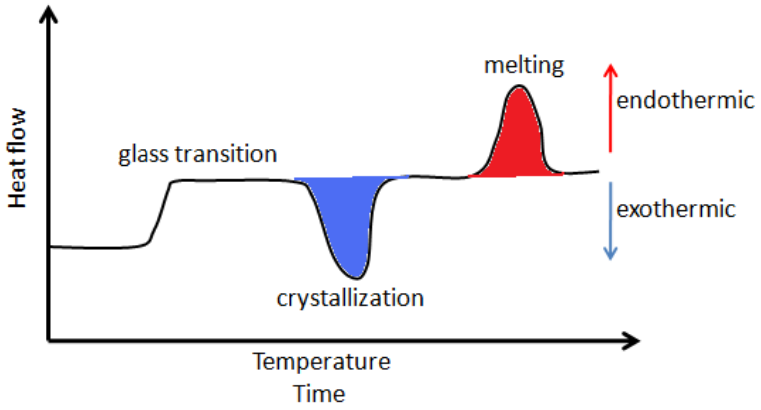

Figure 2-3 A typical differential scanning calorimetry curve can be used to identify various thermal transitions and related heat capacity changes and latent heats.

Differential scanning calorimeters can be designed either as *a heat-flux DSC* or power compensation DSC (Figure 2-4) [Ref 5]. The heat flux DSC belongs to the class of heat-exchanging calorimeters in which exchange of the heat to be measured with the environment takes place via a thermal resistance. In this device, the measurement signal is the temperature difference which is a measure of the heat exchange and is proportional to the heat flow rate. The other type is the *power compensation DSC* in which heat to be measured is compensated with electric energy by increasing or decreasing an adjustable Joule's heat.

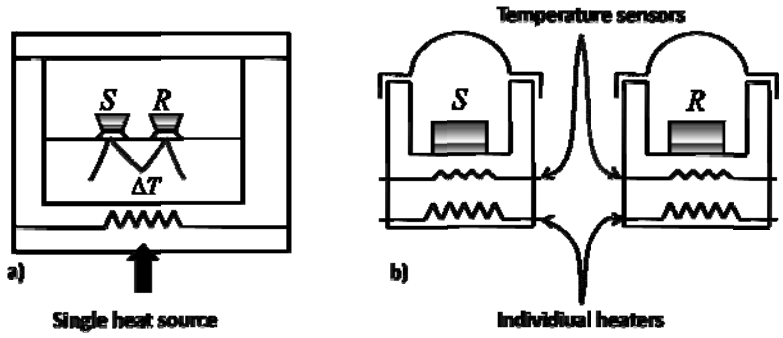

Figure 2-4 Schematic representations of (a) heat-flux DSC; (b) power compensation DSC. S is sample and R is the reference. Both of the calorimeters are twin cell type calorimeters.

2.1.2 Temperature Modulated DSC

Temperature modulated differential scanning calorimetry (TMDSC) is a recent and advanced technique based on the conventional DSC [9]. In TMDSC temperature program is set by superimposing a small sinusoidal temperature oscillation of frequency ω on conventional DSC temperature program [10-12] as

$$T(t) = T_a + \beta t + \chi sin\omega t, \qquad 2.4$$

where T_a is the ambient temperature, (β) is the heating rate, χ is the amplitude of imposed temperature oscillation and $T(t)$ is the instantaneous temperature. In Figure 2-5(a) two DSC curves are given for two different heating rates β_1 and β_2. Glass transition temperature shift with respect to heating rate is indicated with an arrow. But more importantly the increased heating rate β_2 gives rise to an irreversible process as indicated with a dashed circle.

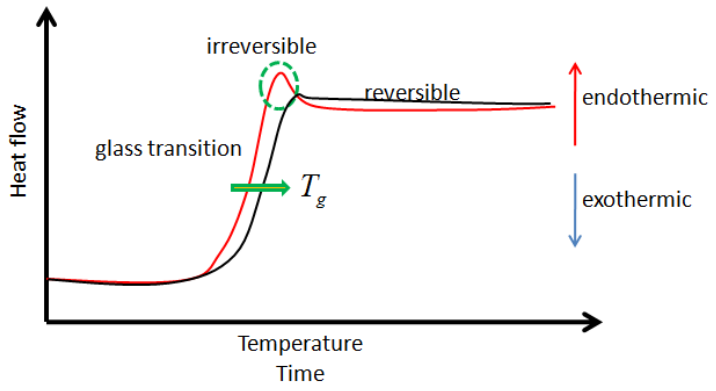

Figure 2-5 DSC curves are given for two different heating rates. T_g is glass transition temperature and glass transition temperature shift is indicated with an arrow.

Sinusoidal temperature modulation as given in Equation 2.4 gives additional analytical tools for further examination of this type of time dependent behavior. While temperature is modulated, the resultant heat flow signal is analyzed using an appropriate mathematical method to deconvolute the response to the modulation $\chi sin\omega t$ from the response of the underlying linear heating

program βt [12]. The different type of contributions to the heat flow can be expressed as

$$\frac{dq}{dt} = C\frac{dT}{dt} + f(t,T) \qquad 2.5$$

where $\frac{dq}{dt}$ is the heat flow into the sample, C is the heat capacity of the sample due to its molecular motions and $f(t,T)$ is the heat flow arising as consequence of a kinetically hindered event. The first term on the right hand side of Equation 2-5 is the reversible part and $f(t,T)$ is the irreversible part. Therefore, MTDSC enables to determine the complex heat capacity and separate reversing processes, such as glass transitions, from non reversing processes such as relaxation endotherms or cure reactions [3, 10]. Hence, identifying glass transition in complex systems becomes easier.

A sample MTDSC curve is given in Figure 2-6 where heat flow, heating rate and the phase between these signals is shown. A peak in the phase is an indication of irreversible processes.

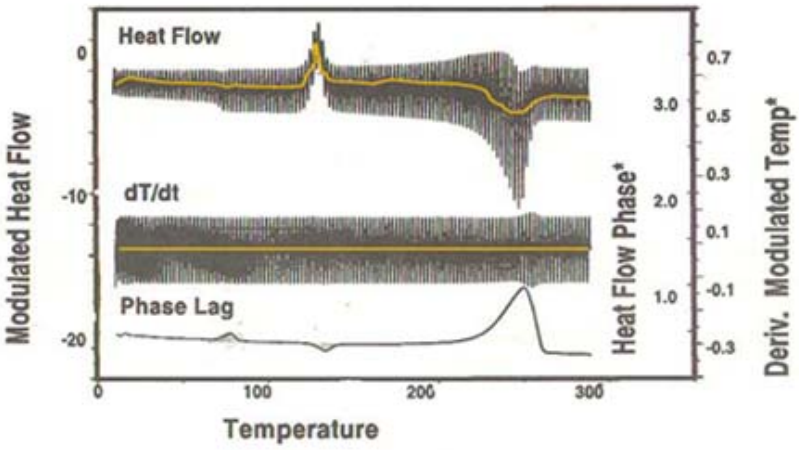

Figure 2-6 Heating rate, heat flow and the phase lag graph of a MTDSC measurement. Average values of modulated heating rate and heat flow are highlighted. After [3].

The irreversible and reversible heat flow signals are deconvoluted by using MTDSC in Figure 2-7. Using the additional phase information obtained from

MTDSC it is possible to differentiate the two heat flow terms in Equation 2-5 as shown in the figure below.

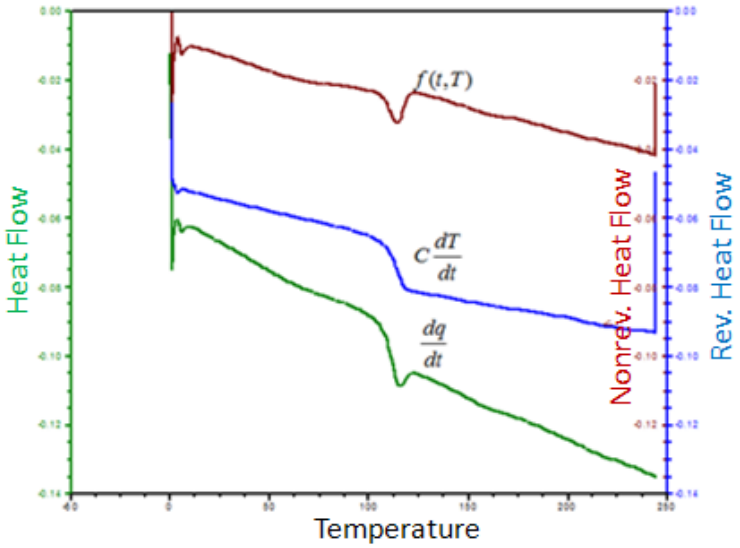

Figure 2-7 The average reversible, irreversible and total heat flow signals of a MTDSC measurement are shown After [13].

2.2 Thermomechanical Analysis

Thermomechanical analysis (TMA) is the measurement of variations in sample dimensions, such as length or volume, as a function of temperature while a mechanical stress is applied. If the applied stress is removed and only effects of temperature are monitored on sample dimensions, the technique is called *thermodilatometry*. In this way thermal expansion coefficients can be determined and variations with respect to temperature and/or time are monitored. The technique determines the coefficient of thermal expansion coefficient of sample from the relationship [3, 4]

$$\alpha l_0 = \frac{\delta l}{\delta T} \qquad 2.6$$

where α is the thermal expansion coefficient, l_0 is the initial length, T is the temperature. Many materials deform under applied stress at a particular

temperature which is often connected with the material melting or undergoing a glass-rubber transition [4]. Figure 2.8 shows a generic TMA curve; thermal expansion coefficient of a glassy material is different before and after the glass transition point.

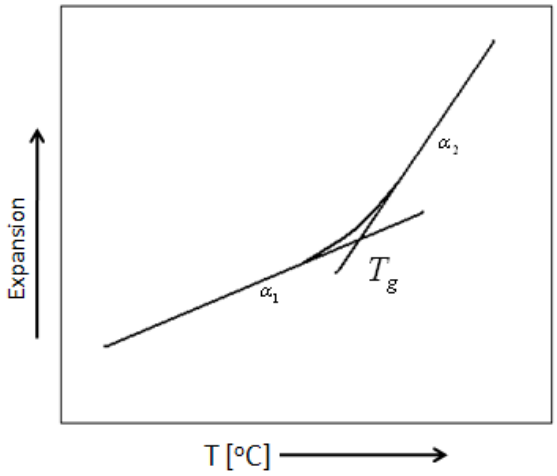

Figure 2-8 A typical TMA curve for a glassy material indicating thermal expansion coefficient change around the Tg, glass transition, point.

2.3 Dynamic Mechanical Thermal Analysis (DMTA)

DMTA is a method for investigating the morphology of materials which can be particularly sensitive to low energy transitions which are not readily observed by differential scanning calorimetry [9]. Many of these low energy transition processes are time-dependent, and by using a range of mechanical oscillation frequencies the kinetic nature of these processes can be investigated. DMTA can be performed either by applying a force initially and monitoring free oscillations while scanning sample temperature or, more frequently, by continuous application of oscillatory force while monitoring oscillations and scanning the temperature simultaneously [4].

The most common DMTA measurement is simply measuring the Young modulus (E) and damping factor against a stepwise increased temperature while an oscillating force at frequency (ω). When the oscillating force

$$\sigma(t) = \sigma_{max} sin\omega t, \quad 2.7$$

is applied to a system the strain response is given as

$$\varepsilon(t) = \varepsilon_{max} \sin(\omega t + \varphi) \quad 2.8$$

where φ is the phase lag between the applied force and the strain response. The complex modulus E^* is given as

$$E^* = \frac{\sigma_{max}}{\varepsilon_{max}} e^{-i\varphi} \quad 2.9$$

where σ_{max} and ε_{max} are the maximum values of applied force and induced strain, respectively. The real part of E^* corresponding to the storage modulus and the imaginary part of E^* corresponding to the loss modulus are given as

$$E' = |E^*| cos\varphi\,, \quad 2.10$$

$$E'' = |E^*| sin\varphi. \quad 2.11$$

The loss factor $tan\varphi$ is a function of the phase between the applied force and induced strain as shown in Figure 2-9.

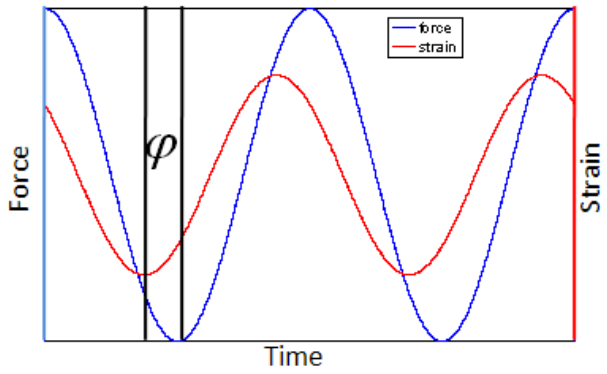

Figure 2-9 The phase relationship between applied force and induced strain for a dynamic mechanical test.

Real viscoelastic materials can be modeled as having the properties both of elasticity and viscosity. For example the Kelvin-Voigt model predicts that the material behavior can be represented by a purely viscous damper and purely elastic spring connected in parallel, whereas for a Maxwell material they are

connected in series. However Maxwell model does not describe creep, and the Kelvin-Voigt model does not describe stress relaxation so a combination of the both models is developed known as the standard-linear material model [14].

In Figure 2.10 storage modulus, loss modulus and loss factor are drawn against temperature. Around the glass transition region, storage modulus decreases and a dramatic change in loss modulus and loss factor is observed.

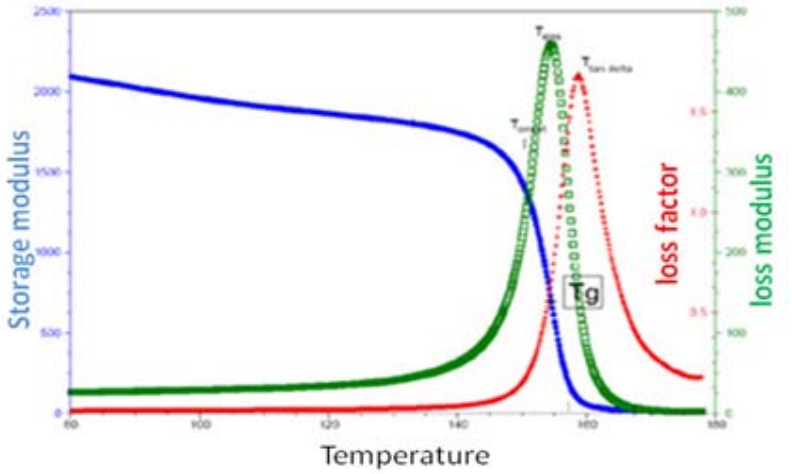

Figure 2-10 Storage modulus, loss modulus and loss factor are shown for a glassy material with respect to temperature. Significant changes occur around glass transition temperature.

Gadaud et al determined the Young modulus and the damping factor of bulk glasses versus temperature using dynamical resonant and subresonant techniques [15-18]. The breakpoints of Young modulus (E) and damping factor (Q^{-1}) versus temperature (T), and resonance frequency of the beam versus temperature (T) curves indicates the glass transition temperature. Figure 2.11 shows the data of the experiment conducted for GeAsSe glass [15].

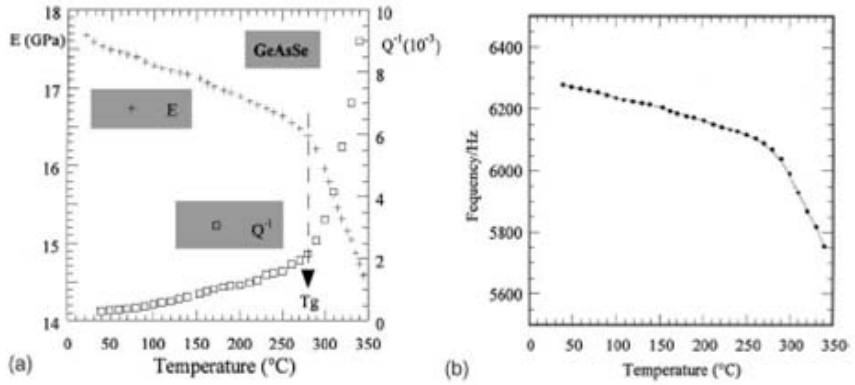

Figure 2-11 (a) Modulus and damping coefficient of GeAsSe glass; (b) corresponding resonance frequency.

2.4 Micro / Nano Calorimeters

The conventional instrumentation for thermal analysis methods, described in the previous sections, enables the characterization of mainly bulk materials. On the other hand, the recent increasing trend towards micro and nano scale systems has brought about the extensive use of small scale materials whose physical properties differ considerably from bulk ones due to the large surface to volume ratio. These property changes include crystal structure changes [19, 20]; melting temperature decreases with respect to bulk values [21-23]; stress relaxation depends on the material size [24-26]. Therefore, to meet the need for the characterization of nanoscale material properties various micro/nano scale thermal sensors that are based on conventional thermo analytical methods have been developed.

For conventional calorimeters, the energy required to heat the calorimetric cell itself (the addenda) would be large compared to either the energy required to heat the sample or the energy involved in the transformation of the sample for samples of small scale. So, the signal of interest would be masked by the contribution from the addenda [27]. Thus, techniques and sensors that are more

sensitive are required. One of the obvious ways to increase the sensitivity is to make the calorimetric cell as small as possible, thus minimizing the effect of addenda.

The developing field of microelectromechanical systems (MEMS) enables the fabrication of ever-small size cell comparable with the size of the sample. Therefore, creation of new characterization probes for the study of material behavior at small scales becomes possible by MEMS technology. By using this technology, various types of calorimetric probes for materials of small scale have been developed [8, 21, 27-38].

L. H. Allen from the University of Illinois at Urbana-Champaign fabricated nanocalorimeters of scanning and differential scanning types and used them for characterization of various small scale materials. The technique used are same as the conventional calorimetry however, by introducing MEMS technology, they decreased the size of calorimetric cells increasing sensitivity that allows small scale calorimetric measurements such as heat capacity, latent heat, transition temperature determination [21, 27-34].

Various other groups used the same technique and similar instrument designs. Vlassak et al demonstrated parallel nano-DSC for combinatorial analysis of nanoscale materials. In this method signal is simultaneously collected from an array of calorimetric cells which is principally based on Allen's design [35].

A novel approach by Gimzewski and Güntherodt is to use the deflection of a bimetallic microcantilever upon heating. For example they measured the phase transition temperatures of n-alkanes placed on the cantilever and associated enthalpy changes with a resolution of 10 nJ [36-38].

2.5 Micro-Thermal Analysis

Micro-Thermal Analysis combines the imaging capabilities of atomic force microscopy (AFM) with localized thermal analysis which is able to measure thermal transitions on a small area of a few square microns. The technique has a

variety of measurement modes, enabling two or more simultaneous measurements [39].

For these analyses, a conventional AFM tip is replaced with a cantilever having a miniature heater/thermometer on it. The cantilever, when used in conjunction with a reference probe, can be used as an ultra-miniature differential scanning calorimeter. Although the total sample is large in comparison to the sensor, probe heats and measures a very small area, a few square microns [40]. Thus monitoring the differential DC power that changes the probe temperature; monitoring the differential AC power and phase gives information about thermodynamic properties of sample resembling DSC and MTDSC results. Since the probe is mounted on the microscope stage, its deflection in the *z*-axis can be monitored during the experiment. This is the microscopic equivalent of the TMA method. Moreover, with this probe DTMA can be conducted if the cantilever is driven by an oscillatory force while the amplitude and phase of the oscillatory movement of the cantilever are monitored [39,40]

Micro/nano calorimeters that have been developed so far are used to determine heat capacity, thermal transitions and associated enthalpies of small scale materials down to picoliter volumes and nanogram mass. There are various types of micro/nanocalorimeters which are available as commercial products [41]. Although available micro/nano calorimeters are reasonably good for measuring thermodynamic properties, they are not integrated with other thermal methods.

Characterization of thermomechanical properties simultaneously with thermodynamical properties is not possible with available micro/nano calorimetry. Separate analysis should be conducted for different properties which is time consuming. In the micro-thermal analysis case, performing various types of measurements simultaneously is possible; however obtaining quantitative information is not possible due to uncertain sample mass. Moreover, heating a very small localized region in a bulk material does not mean nanoscale effects are readily observable.

CHAPTER 2. THEORETICAL BACKGROUND

In the next chapter an analytical model will be developed for a micro thermal analysis probe whose operation principles are based on scanning calorimetry, thermomechanical analysis (TMA), and dynamic mechanical thermal analysis (DMTA).This probe enables thermomechanical and thermodynamical analysis of picoliter volume materials.

Chapter 3

Modeling of System Behavior

The goal of this chapter is to build an analytical model starting from input voltage for obtaining a cantilever deflection formula. The thermal probe described in this thesis is an electrothermally driven bilayer microcantilever which becomes three-layer upon sample placement on it. Applied voltage on the electrical terminals of the cantilever that has finite resistance, reveals power and induces a temperature rise on the cantilever. Induced temperature rise, forces the cantilever to deflect due to thermal expansion coefficient mismatches between constituent layers. This means that energy is converted between three energy domains: (1) electrical domain, (2) thermal domain, and (3) mechanical domain. For the understanding of the cantilever behavior, interaction between these domains should be analyzed. Figure 3.1 shows the system-model-representation that illustrates how energy domains interact.

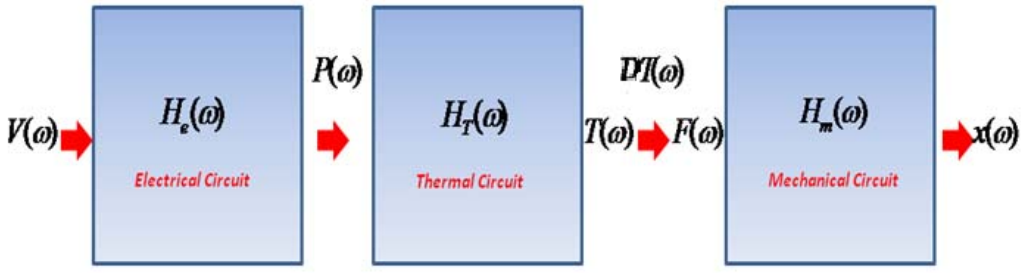

Figure 3-1 System Model Representation of the Cantilever

As Figure 3-1 reveals, combined electrothermal and thermomechanical analysis is necessary for the characterization of the device behavior. Due to easiness of the analysis, circuit-model of the system for each energy domain will be used throughout this chapter [42]. Section 3.1 develops electro-thermal analysis,

Section 3.2 describes mechanical behavior of the cantilever for AC and DC heat loading cases and lastly Section 3.3 describes the overall electro-thermo-elastic behavior of the device for combined DC and AC voltage application.

3.1 Electro-thermal analysis

Joule-heating is the process by which the passage of electrical current through a resistive element releases heat inducing temperature rise on the element. This process can be modeled with the aid of the lumped-element thermal circuit of Figure 3.2 [42, 43].

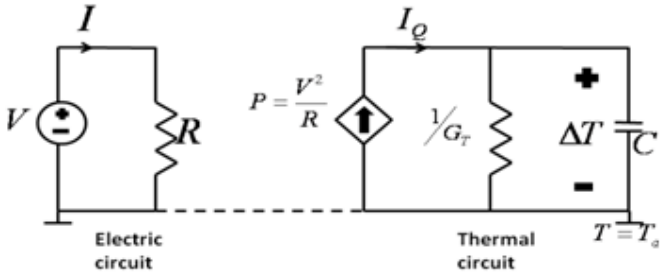

Figure 3-2 Circuit model for the self-heating of a resistor driven from a voltage source.

Consider that the cantilever is initially at ambient temperature T_a, upon heating of cantilever with the voltage generated power

$$P = \frac{V^2}{R}, \tag{3.1}$$

cantilever temperature T increases. Solution of the electric-circuit representation of the thermal model yields the differential equation below, where ΔT ($T-T_a$) is the difference between instantaneous and initial temperature of the cantilever:

$$P(t) = C\frac{\partial \Delta T(t)}{\partial t} + G_T \Delta T(t) \tag{3.2}$$

where C is the total heat capacity and G_T is the total thermal conductance of the cantilever. Heat capacity is material and geometry dependent and given by the formula below for a rectangular m-layer cantilever width of b and length of L where ρ_i, c_i, and h_i are density, specific heat and thickness of the ith layer material, respectively [44].

$$C = (\rho_1 c_1 h_1 + \ \ldots + \rho_m c_m h_m) bL \qquad 3.3$$

Three heat exchange mechanism determine the thermal conductance of the cantilever: (1) Heat conduction between the cantilever and substrate which is assumed ideally at ambient temperature through cantilever materials, (2) heat-exchange between the cantilever and environment by thermal radiation, and (3) heat-exchange between the cantilever and environment by convection. Hence, G_T is the sum of conductive thermal conductance $G_{C,}$ radiative thermal conductance G_R and conductance due to convection G_{cv} [45]:

$$G_T = G_c + G_R + G_{cv} \qquad 3.4$$

G_C and G_R are given as

$$G_C = \frac{b}{L}(h_1 k_1 + \ \ldots + h_m k_m), \qquad 3.5$$

$$G_R = 4bL(\varepsilon_1 + \varepsilon_m)\sigma)({T_a}^3 - T^3). \qquad 3.6$$

where k_i, ε_i are thermal conductivity and emissivity of ith layer material and σ is the Stefan-Boltzman constant (5.67 x 10^{-8} W/m^{2}K).

For analysis of thermal conductance due to air convection Grashof (Gr_L) and Reynold (Re_L) are defined as [46]

$$Gr_L = \frac{g\beta(T-T_a)L^3}{v^2}, \qquad 3.7$$

$$Re_L = \frac{\rho u_\infty L}{\mu}. \qquad 3.8$$

where g, β, T, T_a, L, ν, ρ, u_∞ and μ are the gravitational constant, volumetric CTE, temperature of the cantilever, temperature of the heat sink (i.e. substrate), length between the membrane and the heat sink, kinematic viscosity, mass density, mass average fluid viscosity and viscosity, respectively. For $\frac{Gr_L}{Re_L} \ll 1$ natural convection may be neglected.

Figure 3.3 illustrates how temperature increases respectively with the driven voltage for specific material properties given in table 3.1 where convection is neglected. Temperature increases quadratically with applied DC voltage.

Material	CTE, α (10^{-6} K^{-1})	E(Gpa)	k (W/K.m)	c (J/kg.K)	ρ (Kg/m^3)
Si	2.6	162	149	700	2420
Au	14.3	80	318	130	19400
GAST	14.4	21.9	0.2	130-150	4880

Table 3-1Material Properties

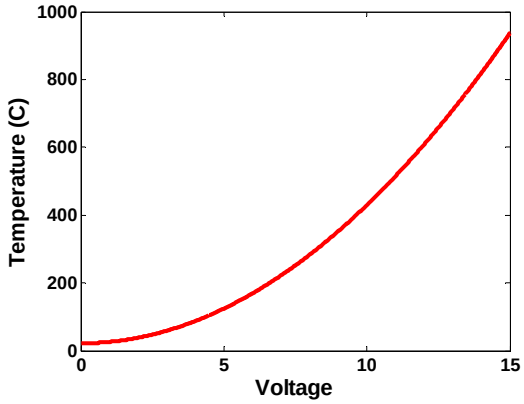

Figure 3-3 Temperature of the Si/Au bilayer cantilever versus applied dc voltage

3.1.1 Thermal Frequency Response upon AC Heating

If the equation 3.2 is solved in frequency domain:

$$P(\omega) = G_T \left(j\omega \frac{C}{G_T} + 1\right) \Delta T(\omega) \qquad 3.9$$

The thermal transfer function can be calculated as

$$H_T(\omega) = \frac{\Delta T(\omega)}{P(\omega)} = \frac{1}{G_T(1+j\omega\tau)} \qquad 3.10$$

τ is the thermal time constant of the cantilever and given as $\tau = \frac{C}{G_T}$. The thermal time constant τ can also be defined as the point where amplitude of the response decreases to 0.707 of its initial value and τ can be obtained from frequency response shown in figure 3.4 experimentally.

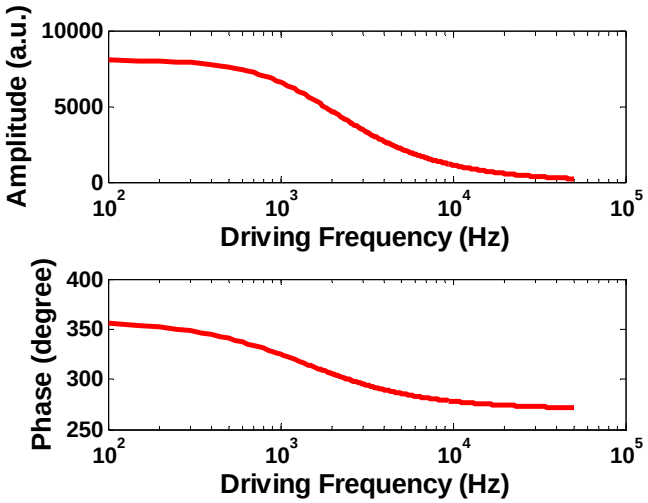

Figure 3-4 Thermal frequency response of the cantilever: Amplitude and phase of the thermal transfer function.

3.2 Thermo-elastic Analysis

Thermoelastic analysis describes the relation between the electrothermal power and cantilever deflection.

3.2.1 Thermal Deflection of Multilayer Structures

A multilayer structure will deflect due to thermal expansion coefficient mismatches of constituent layers when temperature variations occur. In order to obtain a relation between the temperature change and induced deflection, we can decompose the structure to individual layers and apply an effective force F_i and an effective moment M_i to each layer with the sign convention as illustrated in Figure 3-5.

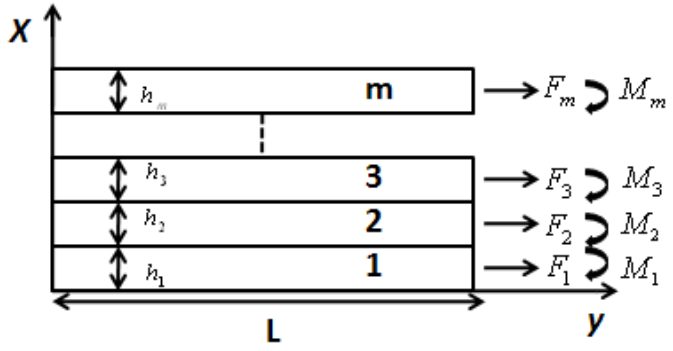

Figure 3-5 One-end-fixed and one-end-free m-layer structure. All layers have same length, L along.

When the static equilibrium is reached all forces and moments should sum up to zero by conservation laws.

$$F_1 + F_2 + \ \ldots \ + F_m = 0 \tag{3.11}$$

$$\sum_{i=1}^{m} M_i + F_1 \frac{h_1}{2} + F_2 \left(h_1 + \frac{h_2}{2}\right) + F_m \left(h_1 + h_2 + \cdots + h_{m-1} + \frac{h_m}{2}\right) = 0 \tag{3.12}$$

From beam theory,

$$M_i = \frac{E_i b {h_i}^3}{12r} \ \ for\ i = 1\ to\ m \tag{3.13}$$

where E_i, h_i are the Young modulus and thickness of ith layer respectively, b is width, and r is the radius of curvature of the beam. Total strains at layer boundaries should be equal, resulting in a set of (m-1) equations:

$$\alpha_i \Delta T + \frac{F_i}{E_i b h_i} + \frac{h_i}{2r} = \alpha_{i+1} \Delta T + \frac{F_{i+1}}{E_{i+1} b h_{i+1}} - \frac{h_{i+1}}{2r} \ \ i = 1 - m - 1 \tag{3.14}$$

where

$$\varepsilon_{t,i} = \alpha_i \Delta T \tag{3.15}$$

is the temperature induced strain;

$$\varepsilon_{f,i} = \frac{F_i}{E_i b h_i} \tag{3.16}$$

is the effective force induced strain;

$$\varepsilon_{m,i} = \mp \frac{h_i}{2r} \tag{3.17}$$

is the moment induced strain and has negative signs at the top and bottom of each layer. The radius of curvature *r* can be obtained by solving Equation 3.12, Equation 3.13 and *m*-1 equations obtained in equation 3.14 simultaneously. Assuming the tip deflection at the free-end of the structure (δ) is small compared to its length L, and then it can be expressed in terms of *r* as

$$\delta = \frac{1}{2r} L^2 \Delta T. \tag{3.18}$$

Since the thermal probing cantilever consists of two-layer and upon placing a sample on it, it becomes three-layer structure; bilayer and three-layer cantilever deflection equations are given. The general equations for *m*-layer are simplified for bilayer case is given as below [46]

$$\delta = \frac{3E_1E_2h_1h_2\,(h_1+h_2)(\alpha_2-\alpha_1)L^2}{(E_1h_1+E_2h_2)\left(E_1{h_1}^3+E_2{h_2}^3\right)+3E_1E_2h_1h_2(h_1+h_2)^2}\Delta T \tag{3.19}$$

Urey *et al* gives the analytical solution for the deflection of a three-layer structure assuming that middle layer is much thicker than the bottom and top layers($h_2 \gg h_1 \; and \; h_2 \gg h_3$) as below [47]

$$\delta = [3E_1h_1(\alpha_2 - \alpha_1) + 3E_3h_3(\alpha_3 - \alpha_2)]\frac{L^2\Delta T}{E_2{h_2}^2} \tag{3.20}$$

Figure 3.6 shows deflection vs. temperature curves for bilayer and three-layer structures for material properties tabulated in table 3.1.

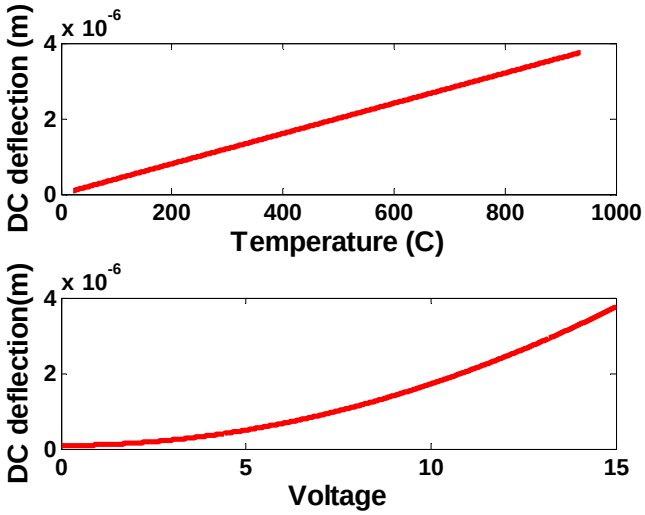

Figure 3-6 DC deflection vs. Temperature and DC deflection vs. DC voltage.

3.2.2 Cantilever Dynamics

The thermal probe is a bilayer cantilever, its one end is clamped to substrate and other end is free. The electrical circuit equivalent of the mechanical system is shown in Figure 3-7. When it is driven with an external force, it can be simply modeled as a damped driven harmonic oscillator and satisfies the nonhomegenous second order linear differential equation

$$m\frac{\partial^2 x}{\partial t^2} + \beta\frac{\partial x}{\partial t} + kx = F_0 \sin(\omega t)\ . \qquad 3.21$$

Here, x is the vertical deflection, m is the mass of the cantilever, β is the velocity-dependent damping constant, and k is the spring constant. The solution to Equation 3.21 is

$$x(t) = A(\omega)\sin\big(\omega t - \varphi(\omega)\big)\ . \qquad 3.22$$

where A is the amplitude and φ is the phase of the oscillation. Both of them are frequency-dependent and are given as

$$A(\omega) = \frac{F_0/m}{[(\omega_0{}^2-\omega^2)^2+\gamma^2\omega^2]^{1/2}} \quad , \tag{3.23}$$

$$\varphi(\omega) = tan^{-1}\left\{\frac{\gamma\omega}{\omega_0{}^2-\omega^2}\right\} . \tag{3.24}$$

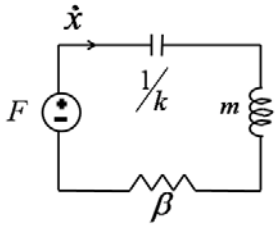

Figure 3-7 Electrical Circuit Representation of The Cantilever as damped, driven harmonic oscillator.

Phase has the opposite signs for $\omega_0 > \omega$ and $\omega > \omega_0$ cases. Here, $\omega_0 = \sqrt{\frac{k}{m}}$ is the first harmonic resonance frequency of the cantilever, $\gamma = \frac{\beta}{m}$ and $Q = \frac{\omega_0}{\gamma}$ is the Q-factor. The maximum amplitude occurs at driving frequency ω_{max} and they are given by

$$A_{max} = \frac{F_0/m}{\gamma(\omega_0{}^2-1/2\gamma^2)^{1/2}} , \tag{3.25}$$

$$\omega_{max} = \omega_0\sqrt{1-\frac{\gamma^2}{2\omega_0{}^2}} . \tag{3.26}$$

The mechanical transfer function relating *x* to *F* is given as

$$H_m(\omega) = \frac{x(\omega)}{F(\omega)} = \frac{1/k}{[1-\omega^2/_{\omega_0{}^2}+j\frac{\omega}{\omega_0}Q]} \tag{3.27}$$

Figure 3.8 shows the mechanical frequency response of a cantilever having resonance frequency of 39.4 KHz and quality factor of 40.

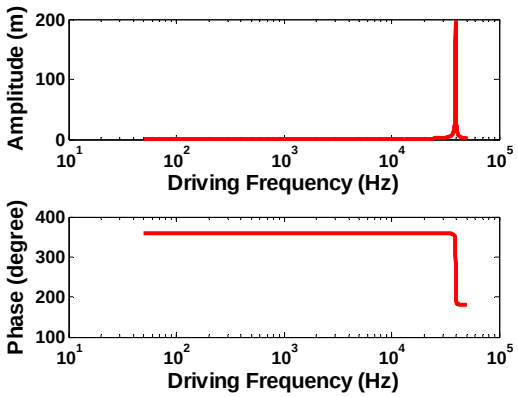

Figure 3-8 Mechanical frequency response of the cantilever: amplitude and phase.

3.2.3 Thermomechanical Response upon AC Heating

If oscillatory heating electrothermal power is applied to the cantilever, the amplitude and phase of the oscillatory deflection of the cantilever can be formalized using the equations

$$F = k\delta = D(E_i, h_i, \alpha_i, L)\Delta T \tag{3.28}$$

where $D(E_i h_i \alpha_i, L)$ is a function of variables relating temperature difference to this difference induced force which drives the cantilever. For bilayer cantilever D is given as

$$D = \frac{3E_1E_2h_1h_2\,(h_1+h_2)(\alpha_2-\alpha_1)L^2k}{(E_1h_1+E_2h_2)\left(E_1{h_1}^3+E_2{h_2}^3\right)+3E_1E_2h_1h_2(h_1+h_2)^2} \tag{3.29}$$

and for three layer cantilever it is given as

$$D = [3E_1h_1(\alpha_2-\alpha_1)+3E_3h_3(\alpha_3-\alpha_2)]\frac{L^2k}{E_2{h_2}^2} \tag{3.30}$$

since interaction relation between thermal and mechanical energy domains is formalized, the circuit model representation of the total thermomechanical behavior of the system is given as in Figure 3-9.

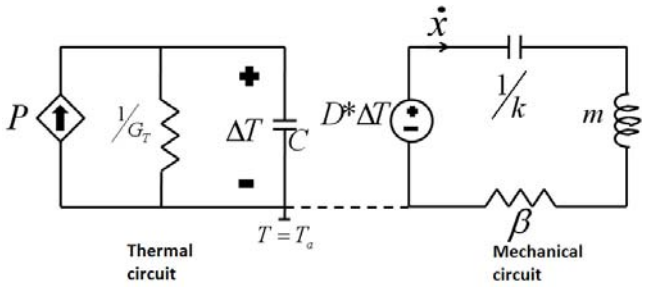

Figure 3-9 The circuit model representation of the thermomechanical system.

Frequency-domain solution of the circuit yields thermomechanical transfer function:

$$H_{TM}(\omega) = \frac{x(\omega)}{P(\omega)} = DH_T(\omega)H_M(\omega) \qquad 3.31$$

Figure 3-10 shows the thermomechanical frequency response of the cantilever which is a combination of thermal and mechanical frequency responses.

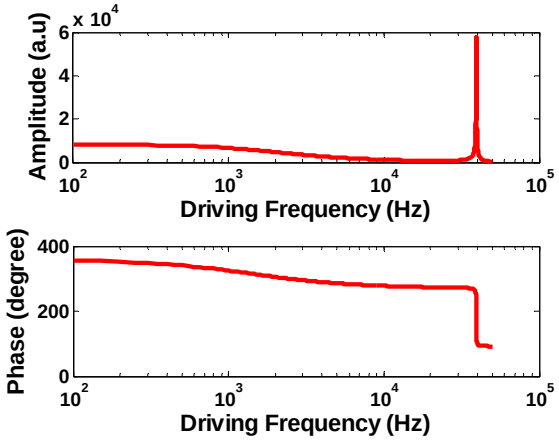

Figure 3-10 Thermomechanical frequency response of the cantilever: amplitude and phase.

3.3 Overall Electro-Thermomechanical Analysis

When combined DC and small signal AC voltage is applied to the cantilever, a small oscillatory deflection superimposed on DC deflection occurs. Application of a voltage

$$V = V_{dc} + V_{ac}\cos(\omega t) \tag{3.32}$$

produces power of

$$P = \frac{2{V_{dc}}^2+1}{2R} + \frac{{V_{ac}}^2\cos(2\omega t)}{2R} + \frac{2V_{dc}V_{ac}\cos(\omega t)}{2R} \tag{3.33}$$

when, there is no sample placed on the cantilever (in the assumption of constituent materials are stable in the given temperature range), temperature and DC deflection of the cantilever induced by the DC component of the power is shown in Figure 3-11.

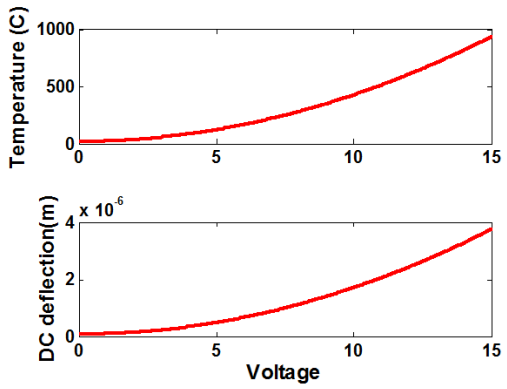

Figure 3-11Temperature and Deflection vs. Voltage of bilayer cantilever.

Figure 3.12 shows the amplitude and phase of the oscillation at frequency ω when vs. V_{dc} when V is applied.

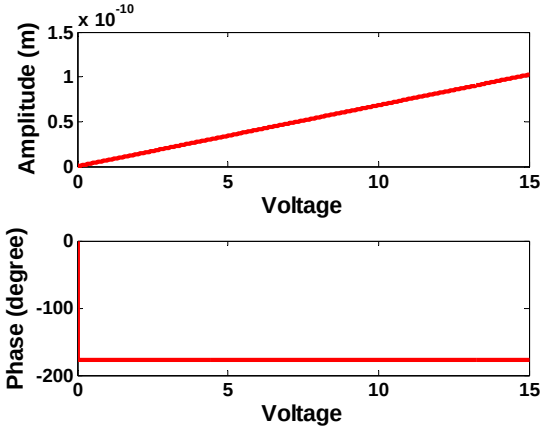

Figure 3-12 Amplitude and Phase of the thermomechanical oscillation at ω vs. Vdc.

If the third layer material placed on the cantilever that has a glass transition (See Figures 3-13a and 3-13b) in the reached temperature range, temperature dependencies of specific heat and Young modulus are formulized by equations below for analytical solutions described in the previous sections. Their variations with temperature are illustrated in Figure 3-15. Figures 3-16 to 3-19 show cantilever response based on this formulization.

$$c_3(T) = c_{3f} - \Delta c_3 \frac{1}{1+\exp\left(\frac{T-T_g}{delT}\right)}. \tag{3.34}$$

$$E_3(T) = E_{3i} + \Delta E_3 \frac{1}{1+\exp\left(\frac{T-T_g}{delT}\right)}. \tag{3.35}$$

E_3 , T_g, and c_3 are Young modulus, glass transition temperature and specific heat of the sample respectively, where i and f subscripts stand for initial and final values of E_3 and c_3 before and after glass transition. ΔE_3 and Δc_3 are differences between initial and final values of E_3 and c_3 respectively and del$T$ defines the glass transition temperature range.

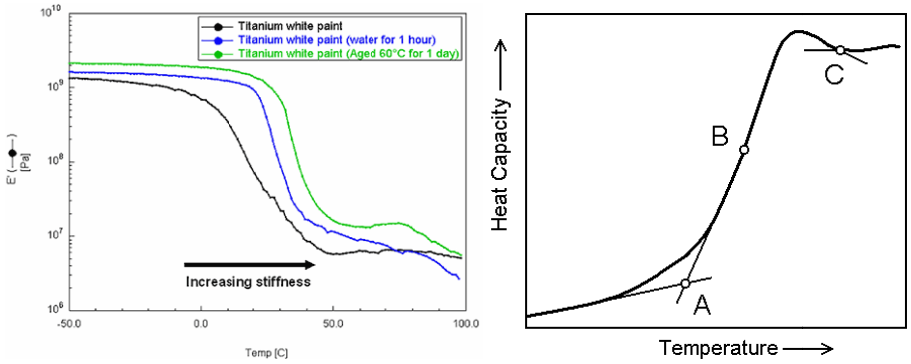

Figure 3-13 a) Young modulus vs. temperature in the range of glass transition temperature b) Heat capacity vs. temperature in the range of glass transition temperature.

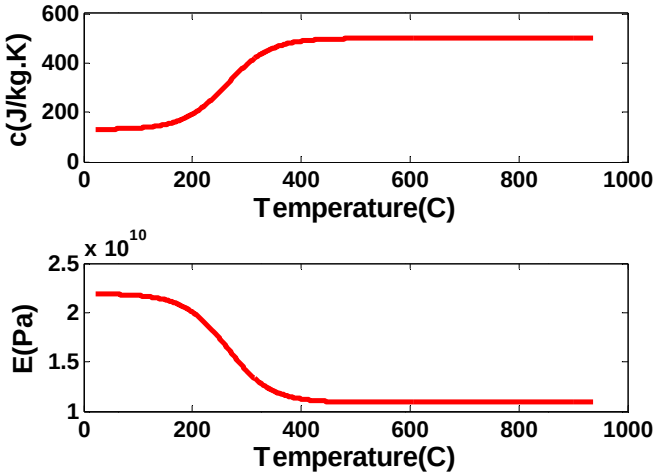

Figure 3-14 Specific heat and Young modulus variation in the glass transition temperature range modeled by eq. 3.20 and 3.21.

In Figure 3.15, variation in resonance frequency is due to Young modulus change of sample layer during glass transition. Quality factor variation is defined in Figure 3.15 based on measurements from literature [15]. When the cantilever is excited thermomechanically at its resonance frequency, amplitude of the oscillation increases linearly with the increasing voltage in the absence of thermal transition events since materials viscoelastic properties do not alter as shown in Figure 3-12. During thermal transition, resonance frequency and Q-factor shift results in deviation from this linear behavior and decrease in the

amplitude and shift in the phase of cantilever vibration driven at its initial resonance frequency thermomechanically as shown in figure 3-17.

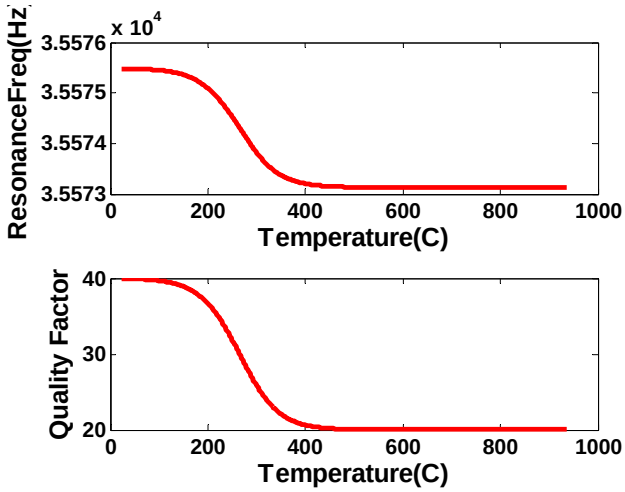

Figure 3-15 Resonance Freq and Quality Factor of Cantilever vs. Temperature.

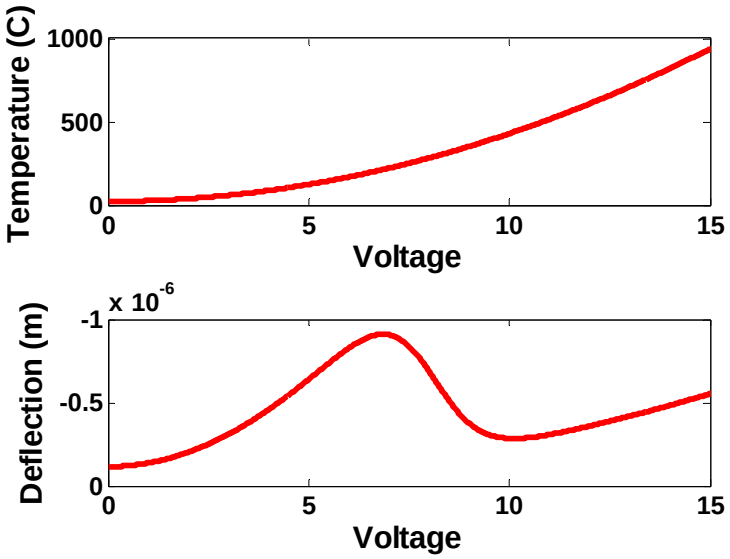

Figure 3-16 Temperature and DC deflection vs. Vdc.in the presence of glass transition.

If the deflection vs. V_{dc} graphs in Figures 3-11 and 3-16 are compared, difference between two graphs is observed. Deflection graph in Figure 3-11

increases quadratically with V_{dc}, where the one in Figure 3-16 deviates from this quadratic behavior due to variation in elastic modulus of the material. There is no obvious difference between two temperature graphs since the addenda ($8.65\times10\text{-}^{8}$J/K) of the cantilever is large compared to sample heat capacity ($3.96\times10\text{-}^{9}$J/K).

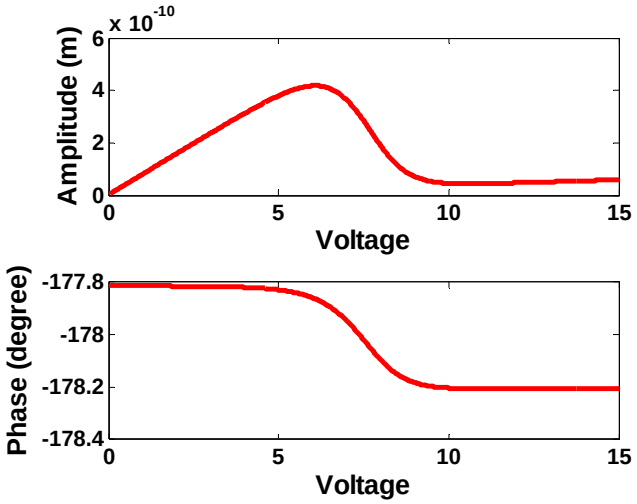

Figure 3-17 Amplitude and phase of thermomechanical oscillation at ω0 vs. Vdc.

If Figure 3-12 and Figure 3-17 are compared in the same manner the deviation from linear behavior of the amplitude is seen which is due to a variation in elastic modulus of the material. Moreover, in the presenece of glass transition a slight decrease in phase occurs which is not seen in Figure 3-12.

If AC voltage is removed and cantilever is driven at its initial resonance frequency mechanically by oscillatory force of 1nN and heated with application of V_{dc} simultaneously, the amplitude and phase of the oscillation will be in Figure 3-18. In the absence of thermal transition, amplitude and phase would be constant since resonance frequency and Q-factor are constant. Variation of frequency and Q results in decrease of phase and amplitude of mechanical oscillation driven at initial resonance frequency of the cantilever.

Amplitude and phase of vibrations at two different frequencies in the range of resonance frequency for the same excitation force yield exact information about variations in resonance frequency and Q-factor of the cantilever with

temperature. Solution of equations below gives the resonance frequency and quality factor. R_i, φ_i are amplitude and phase of the vibrations driven at frequency ω_{di} respectively. F is the mechanical driving force, k is the spring contant that varies also with temperature, and ω_0 is the resonance frequency.

$$\frac{1}{R_i}cos\varphi_i = \frac{k}{F(\omega_{di})}\left[1 - \frac{{\omega_{di}}^2}{{\omega_0}^2}\right] \quad 3.36$$

$$-\frac{1}{R_i}sin\varphi_i = \frac{k}{F(\omega_{di})}\frac{\omega_{di}}{\omega_0 Q} \quad 3.37$$

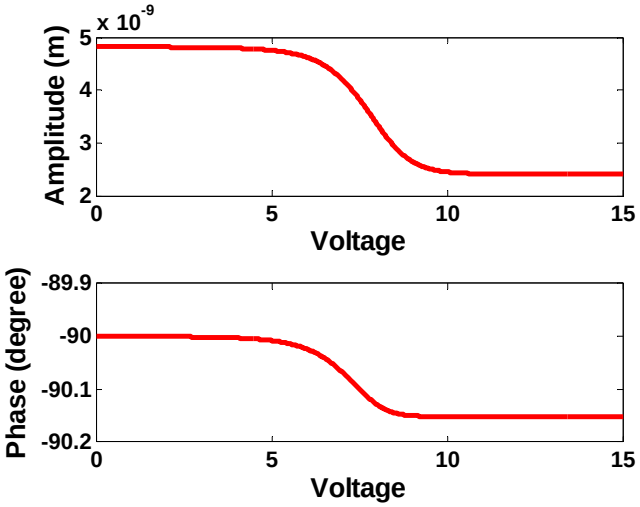

Figure 3-18 Amplitude and phase of oscillation at ω0 driven mechanically vs. Vdc

In summary, this chapter presented analytical electrothermomechanical modeling of two/three layer microcantilever. Starting from applied voltage, heating of the cantilever, DC deflection upon heating, thermal, mechanical and thermomechanical responses are analyzed. Effects of variations in material properties namely young modulus, heat capacity and internal loss on the cantilever behavior are analyzed for comparison with the experimental results presented in the following chapter.

Chapter 4

Device Fabrication, Measurements and Results

In this chapter, firstly fabrication steps for two similar bilayer microcantilever thermal probes are presented. Then, these probes were used for the thermal analysis of thin film chalcogenide glasses As_2S_3 and Ge-As-Se-Te. The thermal excitation and optical measurement setups to detect mechanical deflection and oscillation of the probes are described. Finally, measured deflection, amplitude and phase of the oscillations are presented. In the light of analytical method developed in the previous chapters the observed thermomechanical events are discussed.

4.1 Device Fabrication

Two analogous bilayer microcantilevers thermal probes are used for the thermomechanical analysis. The first type is the SiN_X/Ni bilayer microcantilevers. Hundreds of these microcantilevers, with various dimensions but same geometry, were fabricated on a single chip at the Advanced Research Laboratory, Bilkent University. With these cantilevers, thermomechanical actuation was demonstrated in principle. Although thermal analysis measurements could not be performed with these cantilevers, they still can be used as thermal actuators. The second type of the microcantilevers used is a commercial resistive AFM cantilever of Park Scientific Instruments. This second type is modified by ion beam milling to be used for thermal sensing purposes at the Institute of Materials Science and Nanotechnology, Bilkent University.

4.1.1 SiN_x/Ni Cantilever Probe Fabrication

The first type SiN_x/ Ni bilayer cantilevers are fabricated using conventional bulk micromachining technology. SiN_x and Ni are selected as device materials since they are stable for a vast temperature range and are chemically inert. They are well-known materials in micromachining technology and provide fabrication convenience; fabrication of large arrays of devices is straightforward. Moreover, the large thermal resistance coefficient (TCR) of Ni makes it a good candidate for use as resistive layer since large TCR is advantageous for temperature probing by monitoring resistance variation.

The fabrication of the probe involves the steps of conventional bulk micromachining as shown in Figure 4-1 and are briefly described below.

Wafer cleaning is an essential step for removal of dirt and dust on substrates that may decrease the quality of the films deposited on the substrate thus corrupting device operation. Wafer cleaning was performed by rinsing the wafer with acetone then with isopropyl alcohol (IPA).

Next step is the *SiNx Growth* process. 900 nm SiN_x film is deposited on 110-oriented Si substrate by plasma enhanced chemical vapor deposition (PECVD) system at chamber temperature of 250°C. During the film deposition, SiH_4 and NH_3 gas flows are stabilized to 180 sccm and 22.5 sccm respectively, resulting 10 nm/min film growth rate. This process induces residual stresses in the SiN_x film which causes the cantilevers to bend (Figure 4-4).

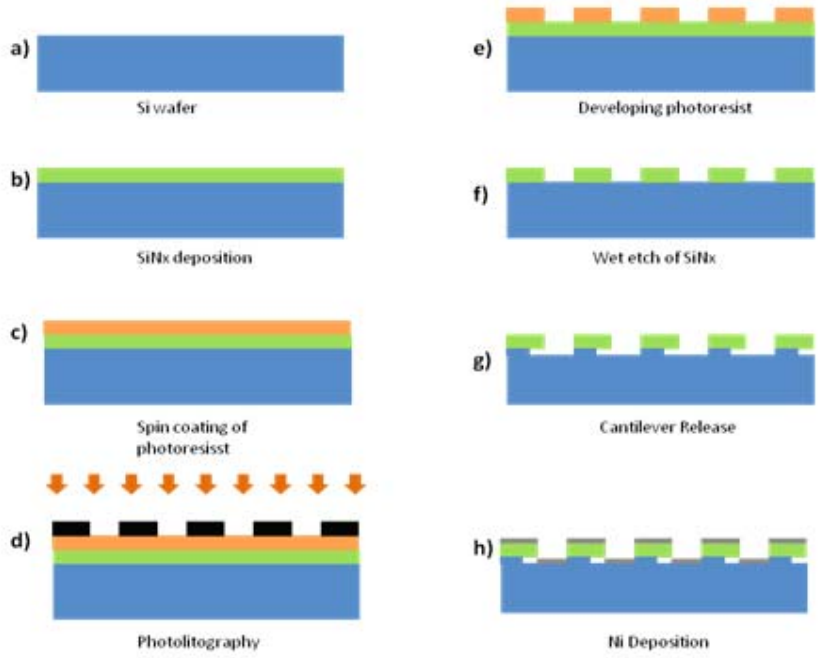

Figure 4-1 SiNx/Ni bilayer cantilever fabrication steps involves conventional bulk micromachining.

Patterning of SiNx; AZ 5214E positive resist is spin-coated on the SiN_x film at 5200 rpm for 40 seconds and soft-baked at 110 °C for 60 seconds. Photolitography step is performed with Karl Suss™ MA-6 mask aligner under 4 mW, 350 nm uv-light illumination for 60 seconds. Mask is turned 45° along the substrate normal for releasing the devices in KOH solution in the following steps of the fabrication process. Illuminated areas of the photoresist are removed by 4:1 DI water/AZ® 400K developer solution. Photoresist is hard-baked at 110 °C for 2 minutes for a better adhesion during etching process. Then, unmasked regions of SiN_x are removed by wet etching by keeping the sample in 1:50 HF/DI water solution for 90 seconds. The resulting patterned SiN_x film is shown in Figure 4-2. After the etching process masking photoresist layer is removed by rinsing with acetone.

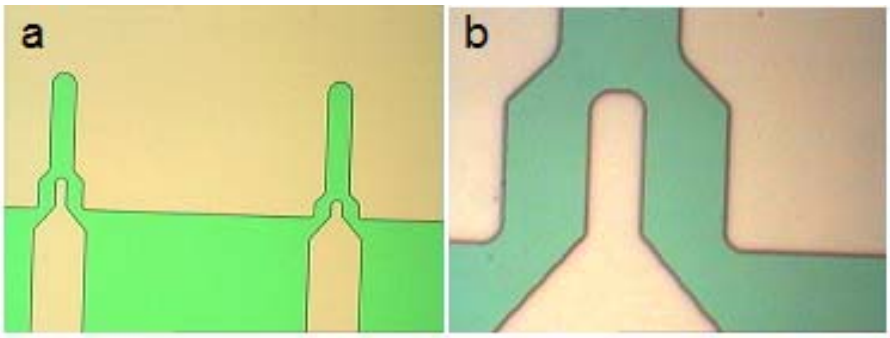

Figure 4-2 Optical microscope images of patterned SiNx films after photolitography and wet-etch processes.

Releasing of Cantilever is performed by removal of the Si substrate material under the cantilever structure by etching with KOH solution. The solution consists of 300 ml DI water and 93 gr KOH. 20 μm gap is formed between the cantilever and the substrate by keeping the sample in 85 °C solution for 55 minutes. Figure 4-3 shows partly released cantilevers at the mid-stage of the releasing process. Yellow-orange color indicates released parts and green indicates unreleased parts of the structure.

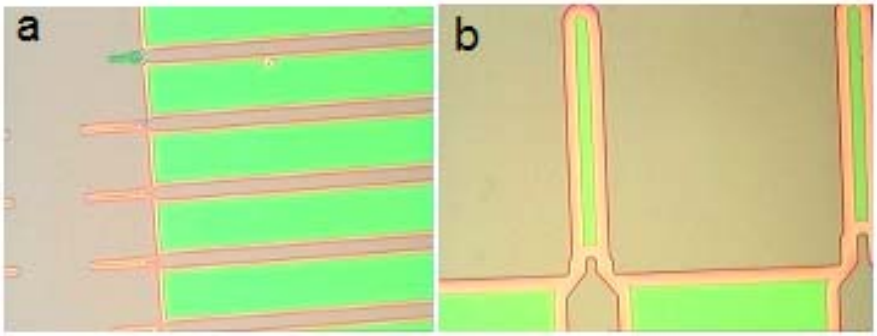

Figure 4-3 Optical microscope images of the cantilevers in the mid-stage of releasing process.

Metallic Layer Deposition; 30 nm Ni layer is deposited as a resistive metal layer by thermal evaporation system, concluding the fabrication process. The metallic layer is used for both joule heating and as a reflector for the optical readout. The scanning electron microscope (SEM) images of the fabricated cantilevers are shown in Figure 4-4.

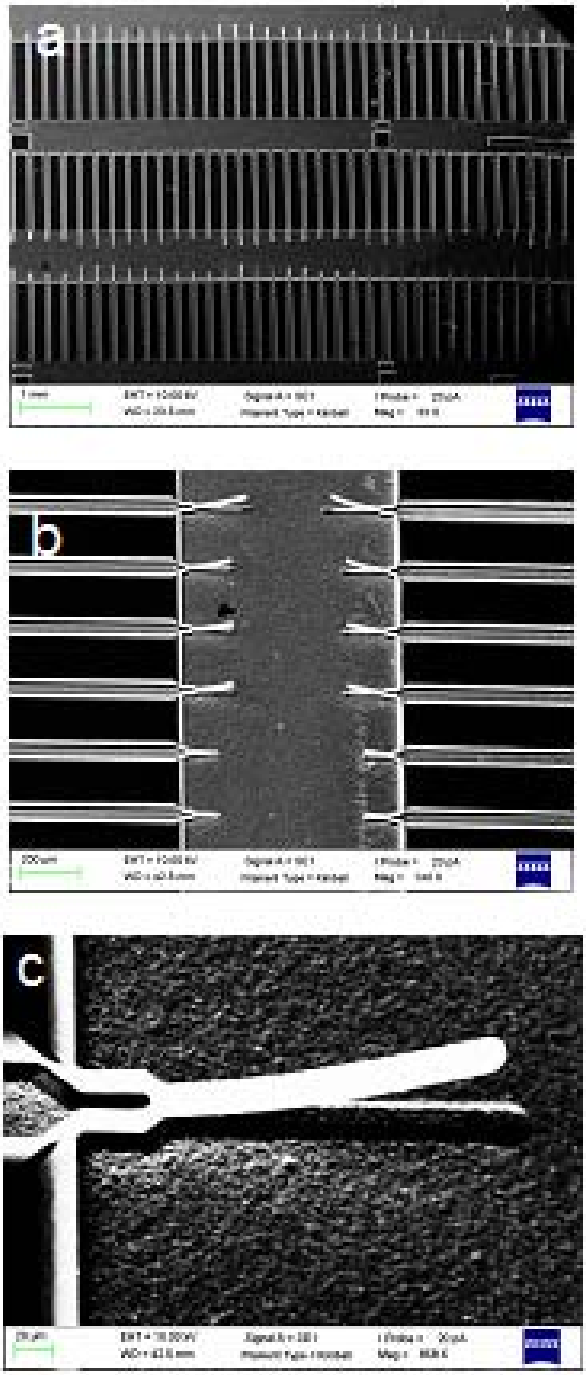

Figure 4-4 Scanning electron microscope (SEM) images of the fabricated microcantilevers. (a)Arrays of cantilevers (b) The contact pads of the cantilevers can be seen clearly. (c) A single cantilever in one of the arrays is zoomed in.

4.1.2 Si/Au Cantilever Probe Fabrication

For an alternative probe design, commercial piezoresistive bilayer cantilevers (Park Scientific Instruments) of 4.5 μm silicon and 0.5 μm Au layers are used (Figure 4.5a). For these cantilevers, at the region of maximum mechanical stress, there is also a temperature gradient involved. The region of maximum mechanical stress is shown in Figure 4-6 to coincide with the temperature gradient on the cantilever as shown in Figure 4-7. In order to increase the sensitivity of the probe, these regions should be separated. For separation a finite element analysis is performed as shown in Figure 4-8 and 4-9. In these graphics, the maximum stress region shifts away from the temperature gradient region. This separation is essential for the validity of equations that describe the thermomechanical behavior of the cantilever derived in sections 3.3 and 3.4; otherwise, in the presence of temperature gradient in the stress region, average values should be used obtained by integration.

This separation of the regions is achieved by 30 kV and 9.3 nA ion beam milling using a FEI Nova Nanolab 600i. Milling regions are defined by MATLAB® code. Final modified cantilevers are shown in Figure 4-5b.

The samples to be analyzed are thin film chalcogenide glasses, Ge-As-Se-Te (GAST), As_2S_3. These thin films are coated on the cantilever surface by vacuum physical vapor deposition (PVD) in a custom-built system. The evaporation rate is stabilized at 10 Å/ s at a base pressure of 5×10^{-6} Torr.

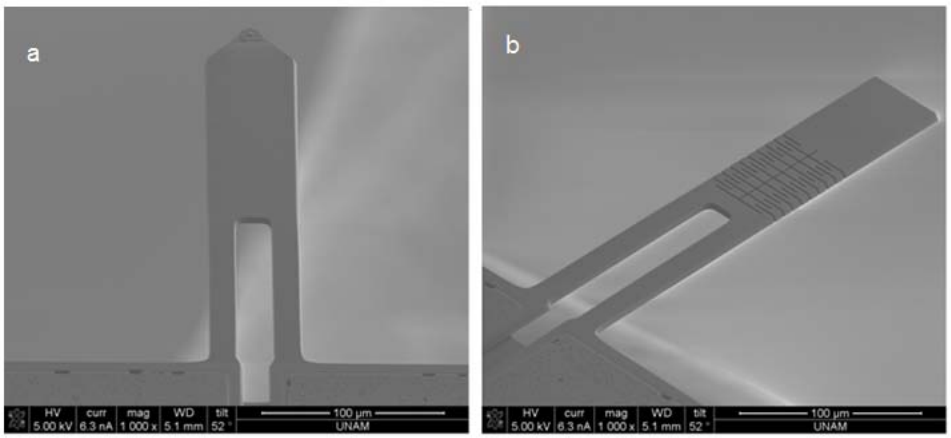

Figure 4-5 SEM images of the microcantilevers (a) before (b) after modification.

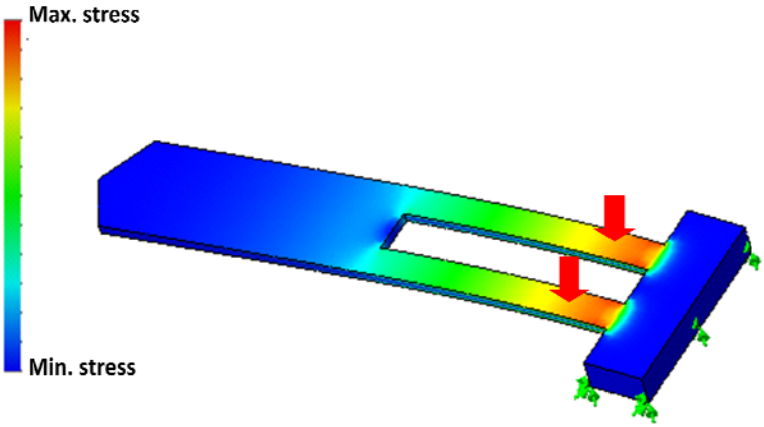

Figure 4-6 Finite element analysis of the first harmonic mechanical mode of the microcantilever before modification. Bending at this harmonic resonance occurs at the regions indicated by the arrows.

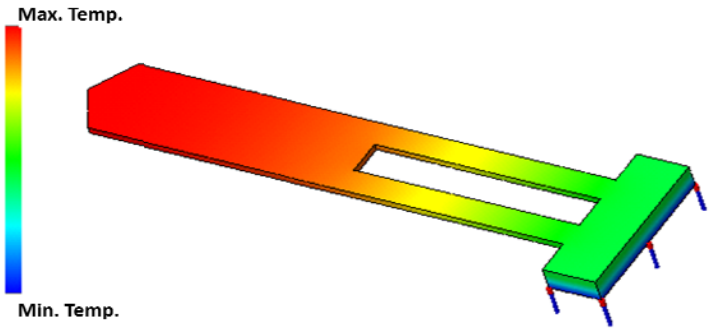

Figure 4-7 Finite element analysis of the temperature distribution before modification of the device. Bending regions cannot reach to maximum temperature and temperature gradient is seen at the bending regions.

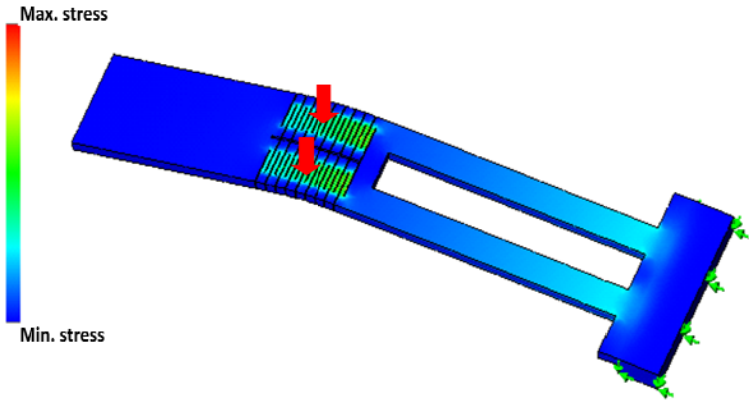

Figure 4-8 Finite element analysis of the first harmonic mechanical mode of the microcantilever after modification. Bending at this harmonic resonance occurs at the regions indicated by the arrows.

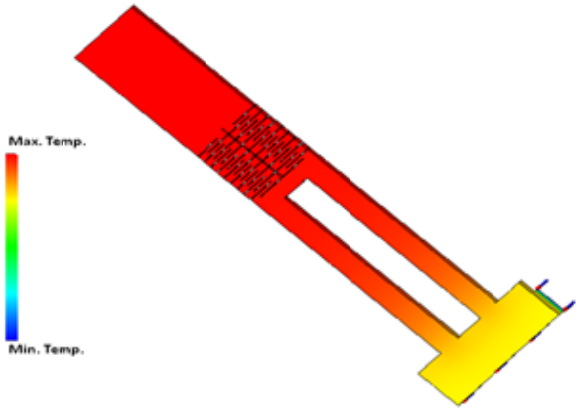

Figure 4-9 Finite element analysis of the temperature distribution after modification of the device. Bending regions can reach maximum temperature and temperature gradient is eliminated at the bending regions.

4.2 Experimental Setup

Mechanical deflection of the both cantilevers is determined optically, *i.e.* the metallic layer of the cantilevers is illuminated by a laser beam and reflected light is measured by a quadrant photodiode as illustrated in Figure 4-10.

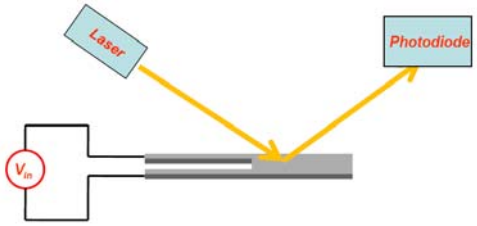

Figure 4-10 Working principle of the microcantilever probe.

SiN_x/Ni cantilevers are driven electrothermally by making contacts with probe station needles to cantilever's contact pads under an optical microscope. They are illuminated on top by a 633 nm LED and reflected laser light is read out by a quadrant photodiode that is placed on the probe station (Figure 4-11).

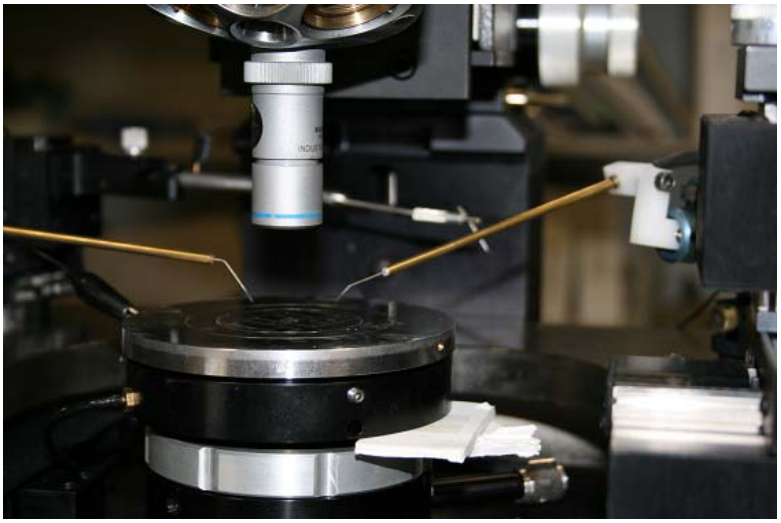

Figure 4-11 Experimental setup for SiNx/Ni cantilever measurements.

Si/Au cantilever is a commercial AFM cantilever; measurements are made using another AFM system (PSIA Advanced Scanning Microscope XE-100E). In order to place the cantilever chip on the AFM head, an extra apparatus is fabricated and the chip is glued on it, see Figure 4.12. The red arrow shows the chip and green arrow shows the apparatus which can be seen better in Figure 4.13. These cantilevers have already macroscopic contact pads on their chips, hence wiring for electrothermal excitation is straightforward, see Figure 4.12. The wavelength of the illumination light is 830 nm.

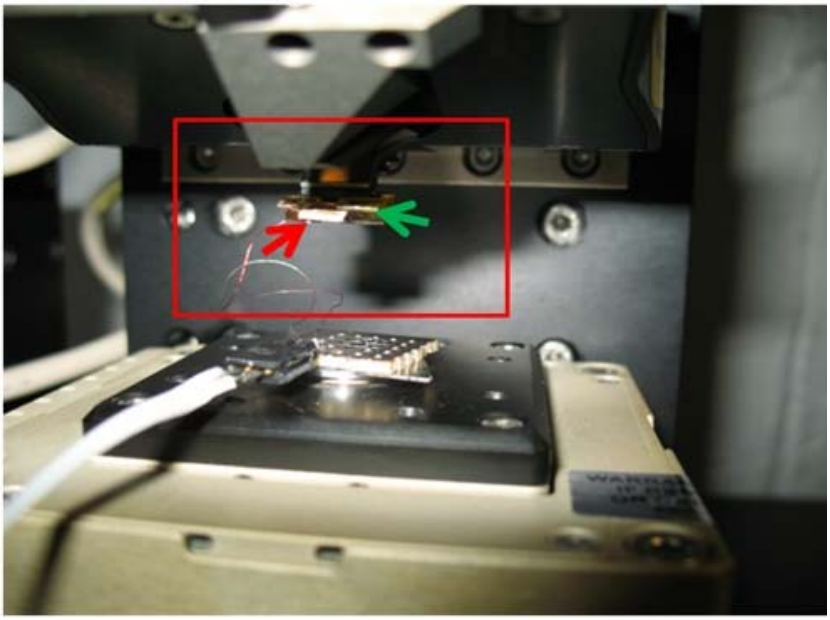

Figure 4-12 Si/Au cantilever placed on AFM head for measurement.

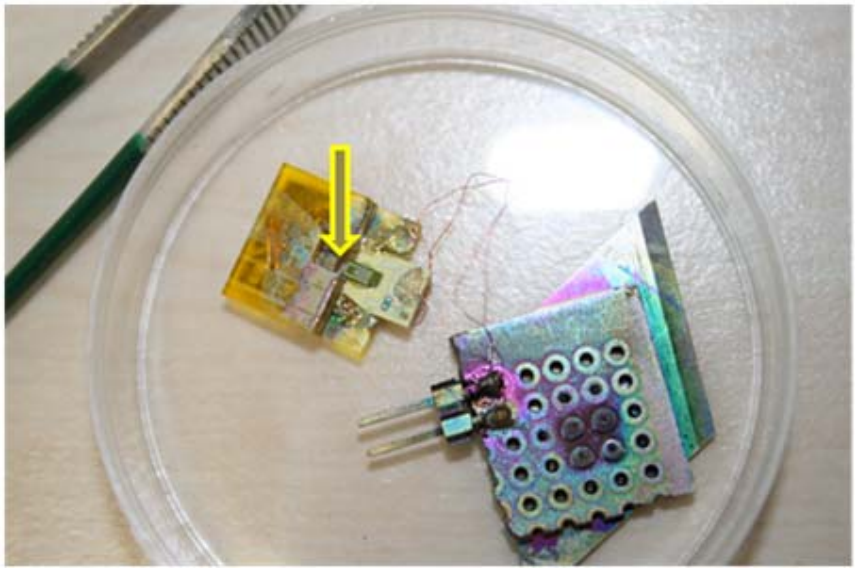

Figure 4-13 A close up view of the cantilever chip.

The complete measurement setup is shown as a flow diagram in Figure 4-14. A function generator (DS345 Function & arbitrary waveform generator, Stanford Research Systems) is used to apply voltage, $V_{dc} + V_{ac}cos\omega t$, to excite the cantilever. A high voltage amplifier is used after the function generator to amplify the voltage. The resulting mechanical deflection and oscillation is measured using laser light that is focused on and reflected from the cantilever tip onto a quadrant photodiode. The photodiode converts the optical signal to electrical signal which is amplified by a low-noise preamplifier (SR560, Stanford Research Systems). The oscillatory signal of frequency ω is then read out by a lock-in amplifier (SR830, Stanford Research Systems). Separately, a computer is used to synchronize the function generator and lock-in amplifier, and also used to record the input and output signals.

Moreover, oscillations at multiple frequencies can be induced by using multiple function generators using an adder circuitry and corresponding signals can be read out by multiple lock-in amplifiers in the same manner.

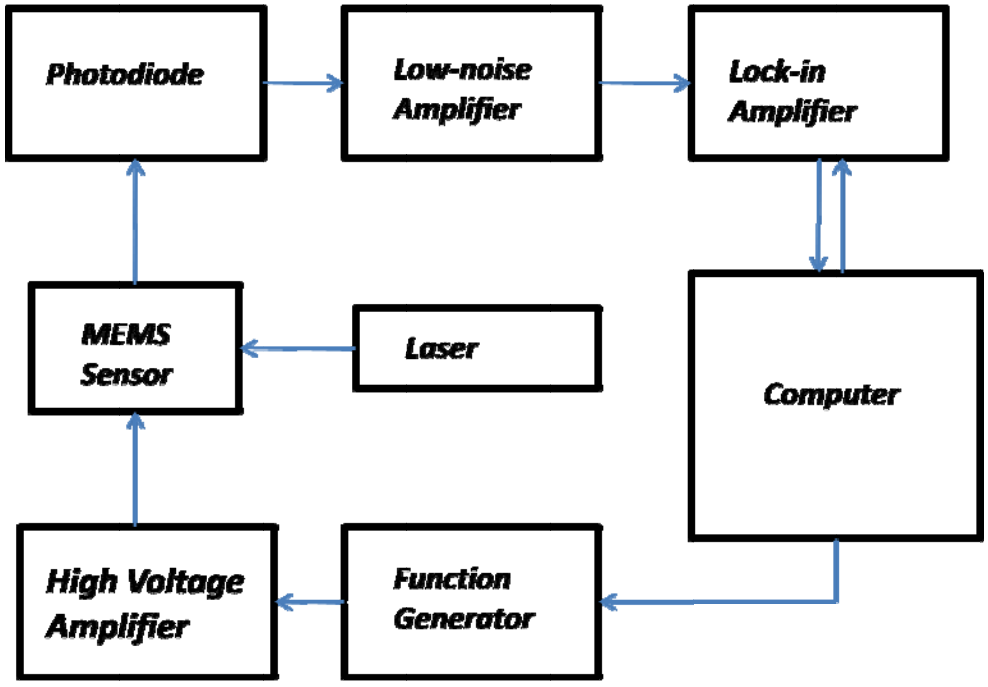

Figure 4-14 Electrical and optical components of the thermomechanical measurement setup.

4.3 Results and Discussion

Thin film characterization and device performance measurements are performed in the following order. Firstly, without sample, frequency spectra of the thermomechanical response of both cantilevers are measured. Time constants, resonance frequencies and quality factors of the cantilevers are obtained. Next, by changing the applied DC voltage that heats the cantilever the shift in resonance frequency and quality factor, obtained in the first step, was observed. Lastly, a linearly increasing DC voltage and a small sinusoidal voltage superimposed on it is applied and DC deflection, amplitude and phase of the mechanical oscillation are monitored. In contrast to stepwise voltage increment, this last step enables to resolve time-dependent character of material properties.

4.3.1 Thermomechanical Excitation and Thermal Time Constant Determination

Electrothemomechanical excitations of both cantilevers at their resonance frequencies which are far beyond their thermal time constant are demonstrated. Measured data fits well to the theoretical model described in Chapter 3 for SiN_x/Ni cantilevers and Si/Au cantilever. From the mathematical fit procedure, different thermal time constants, resonance frequencies and quality factor values are determined. These properties are tabulated in Table 4-1 for various SiN_x/Ni cantilevers with different dimensional lengths. As the length of the cantilevers increase the resonance frequency is observed to shift to lower values.

Cantilever no	Length(L) (μm)	Width(b) (μm)	Leg Length(l) (μm)	Leg width(w) (μm)	Thermal time constant (τ) (μs)	Resonance frequency f_0 (Khz)	Q
1	31	11	24	8	227.3	77.82	30
2	56	11	24	8	281.2	35.96	23
3	86	11	19	8	175.5	27.34	23

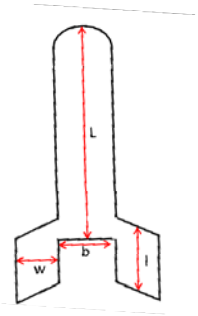

Table 4-1Thermal time constant, resonance frequency and Q values for SiNx/Ni cantilevers having different dimensional lengths which are shown next to the table.

Figure 4.15 shows the thermomechanical responses of these microcantilevers. Blue and red curves show thermomechanical response where green curve is the thermal response.

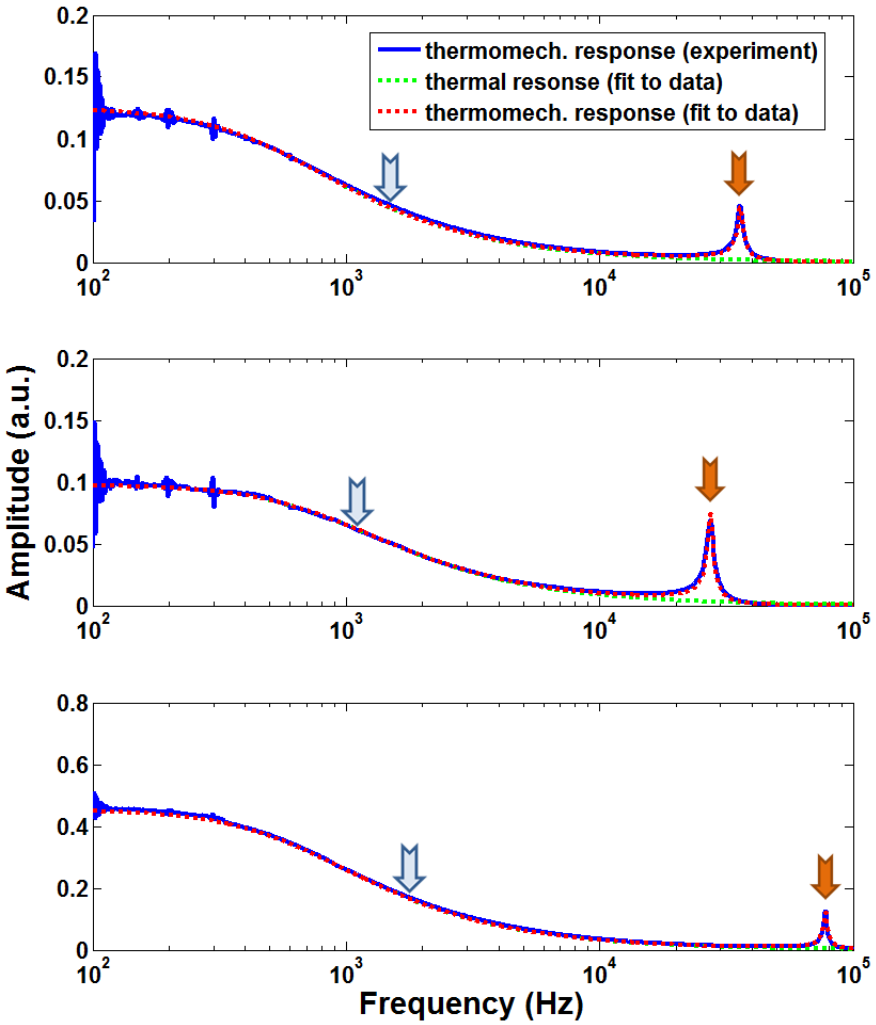

Figure 4-15 Thermomechanical response of SiNx/Ni cantilevers. Time constants and resonance frequencies are indicated.

Also, the thermomechanical response for the Si/Au cantilevers are given in Figure 4-16. Time constant and resonant frequency is marked in the curve. This cantilever exhibits high Q-factor (220) in contrast to the SiN_x/Ni cantilevers.

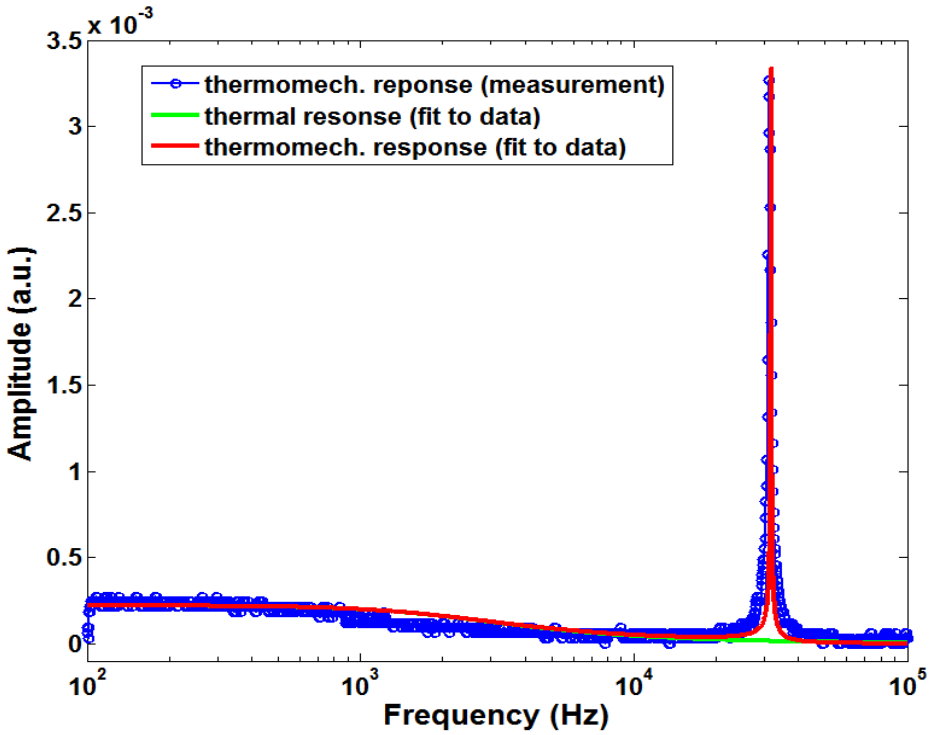

Figure 4-16 Thermomechanical response of Si/Au cantilevers with a considerably high Q value of 220. Time constants and resonance frequencies are indicated.

4.3.2 Effects of Temperature on the Resonance Frequency and Quality Factor

Increase of temperature induces variations in the Young modulus and viscosity of the material therefore resonance frequency and quality factor of the microcantilevers, which dependent on the material properties, shift as described previously in Chapter 3. To determine how these changes occur, frequency spectrum of the cantilever, with a 100 nm Ge-As-Se-Te glass, is measured for different DC voltage values resulting in different temperature. This was done in the range of first harmonic resonance frequency. Figure 4-17 shows amplitude and the phase of the thermomechanical oscillations versus frequency. From the figure, the shift of the resonant frequency to the lower values can be seen. This shift is combined with an increase of the amplitude because of DC heating; this

is followed by a decrease due to the further frequency shift. This is a typical example of a dynamical mechanical thermal analysis (DMTA).

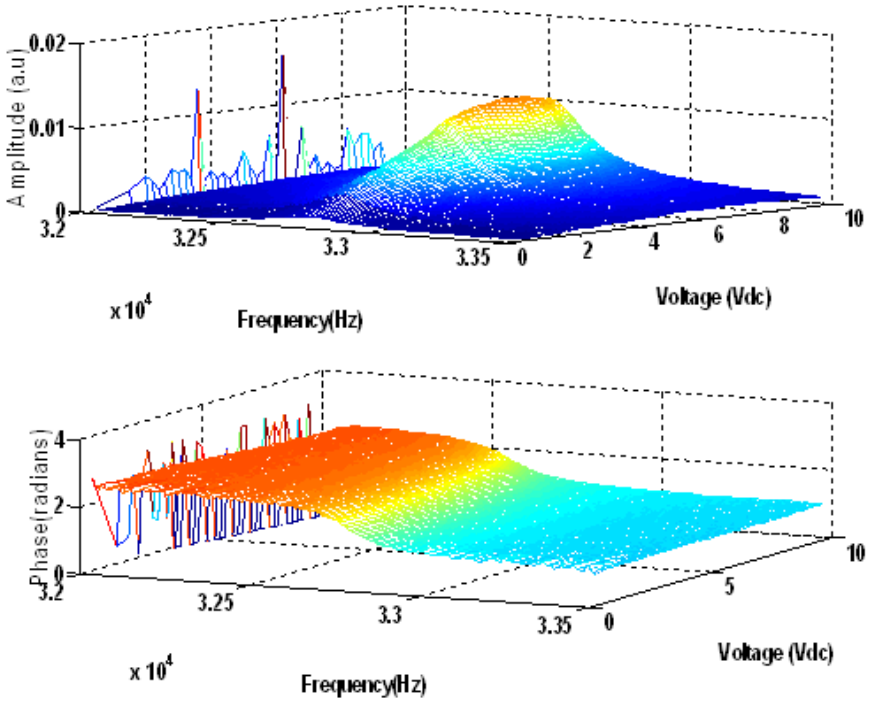

Figure 4-17 Amplitude and phase of the thermomechanical oscillations versus frequency and V_{dc}.

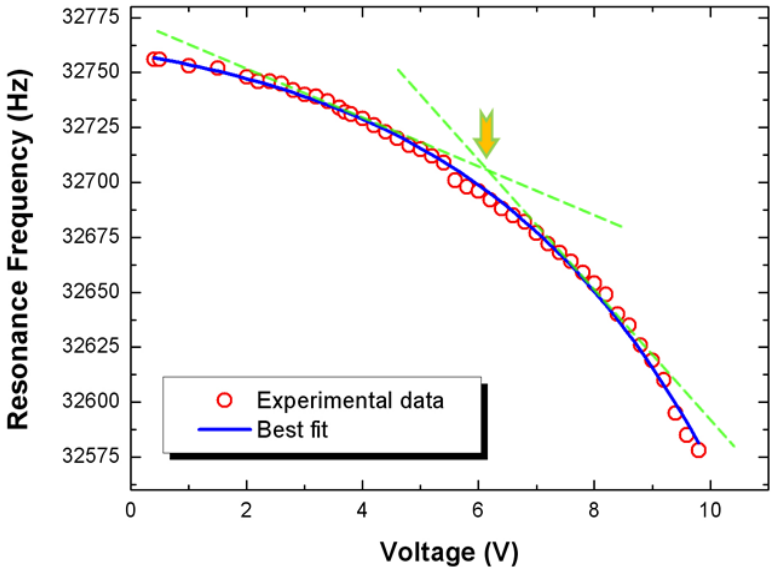

(a)

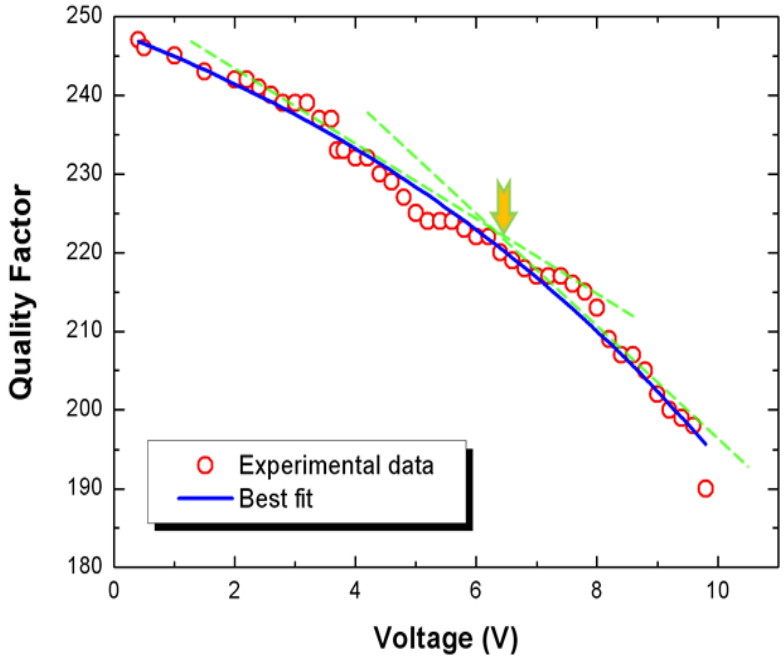

(b)

Figure 4-18 (a) Resonance frequency of the microcantilever with Ge-As-Se-Te sample on it versus Vdc (b) Q-factor of the same microcantilever.

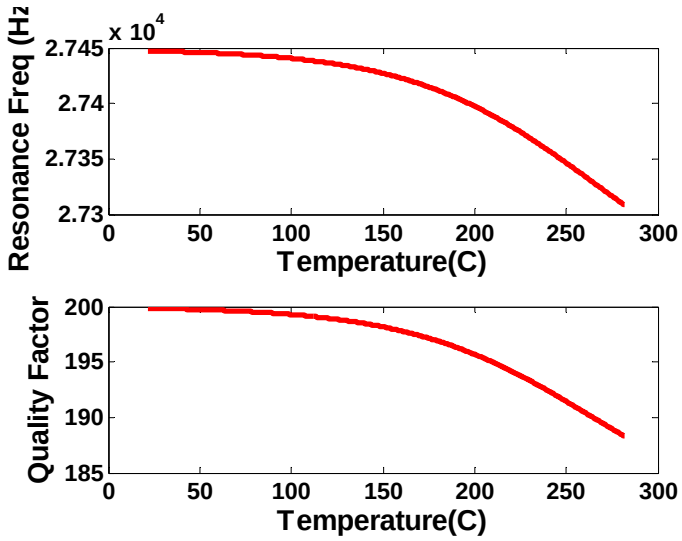

Figure 4-19 Analytical model of resonance frequency and Q-factor variation which shows the same behavior with experimental results.

Figure 4-18a and 4-18b show resonance frequency and quality factor versus DC voltage. This is obtained by fitting model parameters to the data shown in Figure 4-17. As illustrated in Figure 4-18a and 4-18b, both of the graphs can be decomposed into two linear regions with different slopes, indicated by green lines. The joint points of these lines, indicated by red arrows, are indicators of a thermal transition point, *i.e.* glass transition point of Ge-As-Se-Te glass sample. The characteristics of the graphs are similar to those found in literature [15, 18] and to the ones obtained from the analytical model, see Figure 4-19.

However, there remains a problem with this kind of frequency spectrum measurement. During the measurement, which takes approximately a minute, DC voltage of specific value is applied to the device continuously, raising its temperature unless it reaches steady state. Hence, during frequency spectrum measurement temperature may alter which should be avoided. For this case, temperature reaches steady state before reaching resonance frequency range which is clear in Figure 4-17. Nevertheless, this method is not feasible for a vast temperature range since it would be time consuming to scan resonance frequency range which is not always clear due to thermal transitions for each temperature value.

4.3.3 Deflection and Thermomechanical Oscillation Amplitude and Phase

From the above discussion it is clear that simultaneously increasing DC voltage and monitoring resonance frequency are not possible. Therefore another method should be used. Monitoring DC deflection and thermomechanical oscillation amplitude and phase driven at a specific frequency enables gathering continuous information for a specific V_{dc} range and thus a continuous temperature range.

The cantilever was excited by the

$$V = V_{dc}(t) + V_{ac}cos\omega_0 t \tag{4.1}$$

where

$$V_{dc}(t) = \beta t. \tag{4.2}$$

For one measurement cycle, during the first ten seconds β is positive whereas in the next ten seconds it is negative; thus completing the cycle. In Figure 4-20, force versus voltage curves for multiple measurement cycles of different β values ranging from 0.075 V/s to 1.5 V/s are shown. For this measurement force corresponds to the deflection of the cantilever.

In the temperature range where material properties are stable, the deflection curve, or force curve in this case, should be a quadratic function of the DC voltage applied as discussed in Chapter 3. The deviation from this behavior indicates a material property change.

Up to a certain β value, although a small deviation from the quadratic behavior occurs, the deflection increases with increasing DC voltage. After a certain β value, the deflection does not increase anymore with further increasing DC voltage. As the β value further increases same effect occurs at a higher DC voltage. This is due to the time dependency of the thermal event occurring that changes the material properties. This behavior is described in Section 2.2 and shown in Figure 2-1 in detail.

Upon further examination of Figure 4-20, more interesting features can be recognized. The hysteresis between positive and negative measurement cycles

is attributed to the *irreversible* part of the thermal process that happens at the same time with glass transition which is itself a *reversible* process. The difference of the hysteresis area for subsequent measurement cycles is remarkable. In general higher β rates result in larger hysteresis area. This irreversible part disappears after a few measurement cycles; since the deformation of the material is complete.

The same hysteresis area difference can also be seen from Figure 2-1; the area increases with increasing β rates but does not stop. This is due to the fact that each measurement scan is repeated for a different fresh sample.

A distinct thermal event, evaporation, was also observed upon further DC voltage increase. This is less subtle than the glass transition since mass loss affects the cantilever's mechanical behavior dramatically. The bold blue curve is the positive part of a measurement with β=1.5*V/s* whereas the bold red is the negative part of the same measurement cycle. Evaporation occurs at the end of the positive cycle and finishes at the beginning of the negative cycle completely changing the behavior of the force curve. Dashed curves are the positive and negative parts of the next measurement cycle that has the same β value with the previous one. Dashed curves exhibit the same characteristic with each other and with the negative part of the previous cycle. Also note after evaporation, the force curve shows no hysteresis. The evaporation of the sample from the cantilever tip is also photographed and shown in Figure 4-22. The fact that As_2S_3 film remains on the parts of cantilever closer to the heat sink agrees with the FEA simulation.

Up to this point, the DC deflection is explained corresponding to the DC power. At the same time with the DC deflection, amplitude and the phase of the oscillations corresponding to AC power of frequencyω_0, are measured. This also gives ample information about the process and supports the information obtained from DC deflection. In Figure 4-21 amplitude and phase curves of the same measurement cycles defined in the previous discussion are shown. The deviation of the amplitude curves from its initial linear behavior is an indication

of glass transition point T_g which depends on the heating rate β [10]. T_g can also be observed from the smooth decrease of the phase. For the phase curves, T_ω reveal another ergodicity breaking point like T_g associated with modulation frequency, ω_0. At T_ω point, the phase signal has a peak [10]. In the analytical model, only the slight change in phase is predicted associated with T_g, however the model does not predict the peak because material's time dependent response is not included. By including the material models, described in Chapter 2, this behavior can be integrated into the theoretical model.

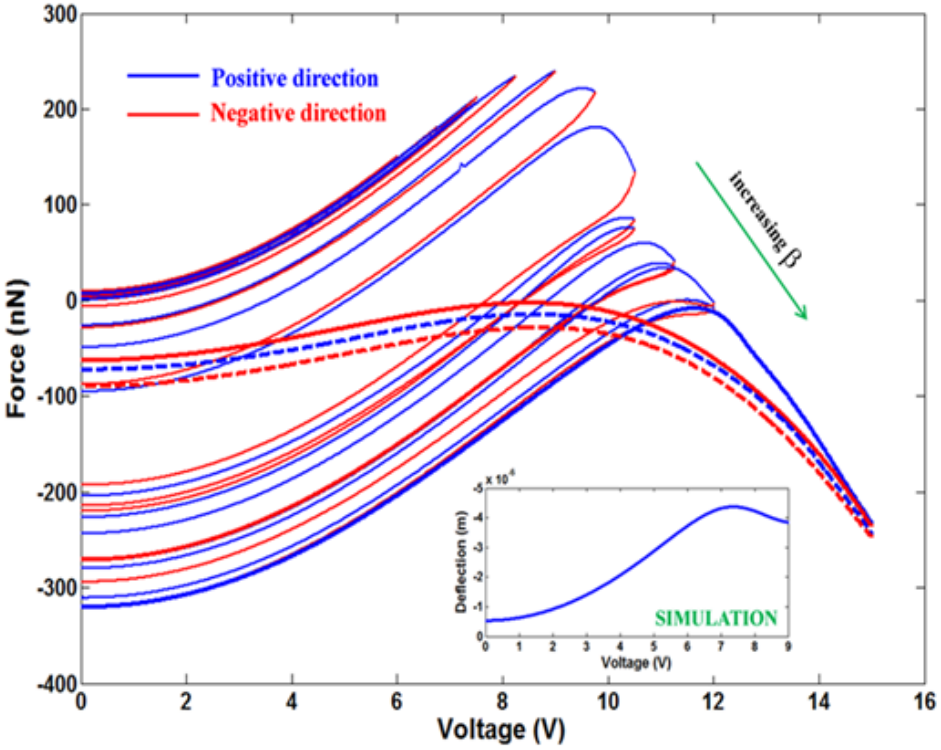

Figure 4-20 Force vs. Vdc curves of measurement cycles with different heating rates. The sample used is 100 nm thick As2S3 film. Inset shows the analytical model curve for DC deflection vs. Vdc.

On the other hand, the irreversible thermal processes cannot be readily observed from these curves. Evaporation event can be observed from both curves using the same reasoning described above. After evaporation, behavior of the

amplitude curve is linear and deviation from this curve does not occur. That is the case where material properties do not alter with temperature illustrating stability of probe materials against temperature.

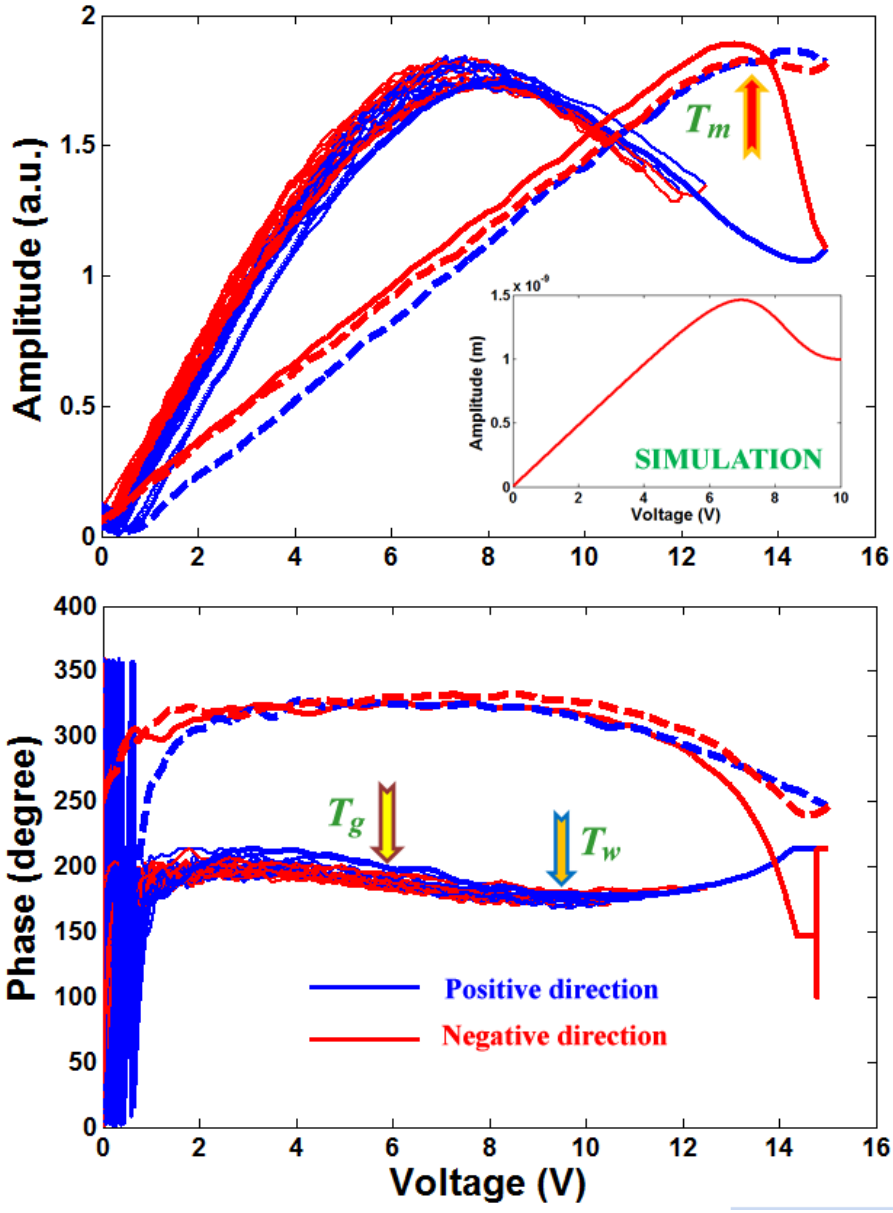

Figure 4-21 Amplitude and phase of thermomechanical oscillation driven at resonance frequency. Inset shows analytical model response which is in agreement with measurement characteristics.

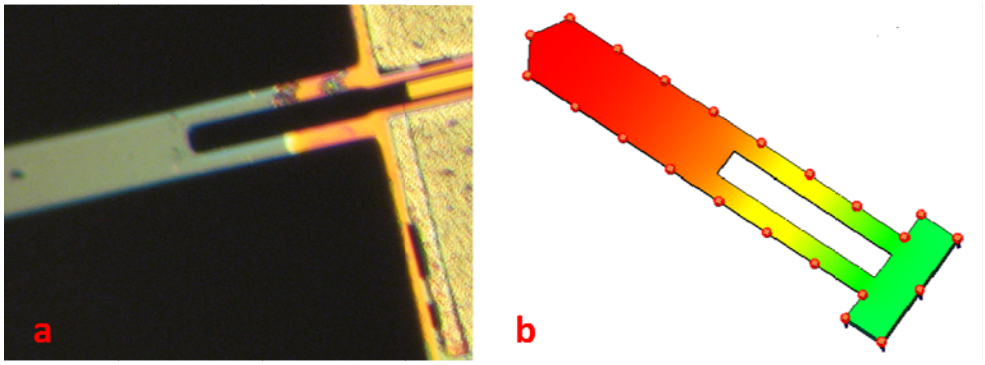

Figure 4-22 (a) Optical image of the device after measurement. Evaporation of sample material is seen. (b) FEA simulation showing temperature distribution on the device.

Similar measurements are conducted with 100 nm Ge-As-Se-Te thin film sample for just one measurement cycle. Figure 4-23 and Figure 4-24 show the force response and amplitude and phase responses, respectively. T_g and T_ω are also observed in this measurement and are indicated in the figures.

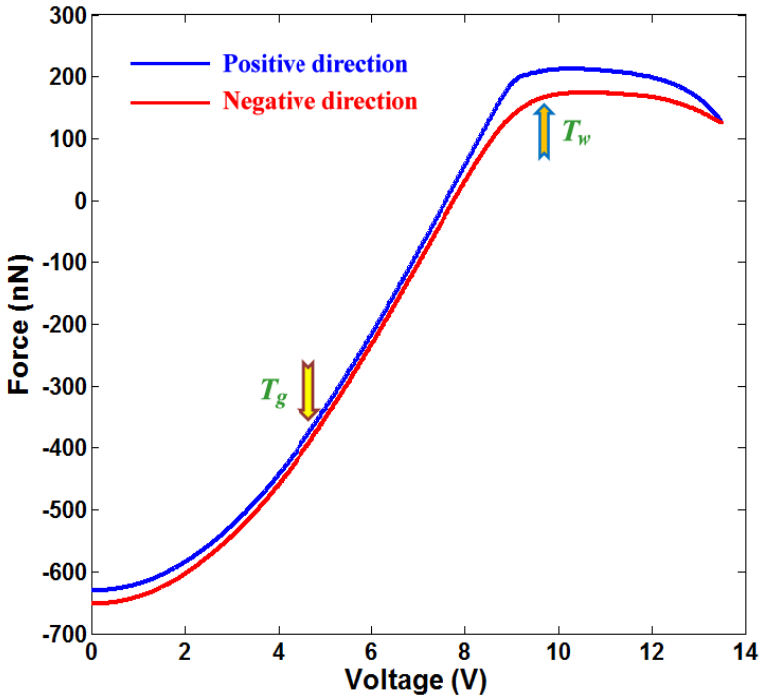

Figure 4-23 Force vs. Vdc curves of one measurement cycle. The sample used is 100 nm thick.

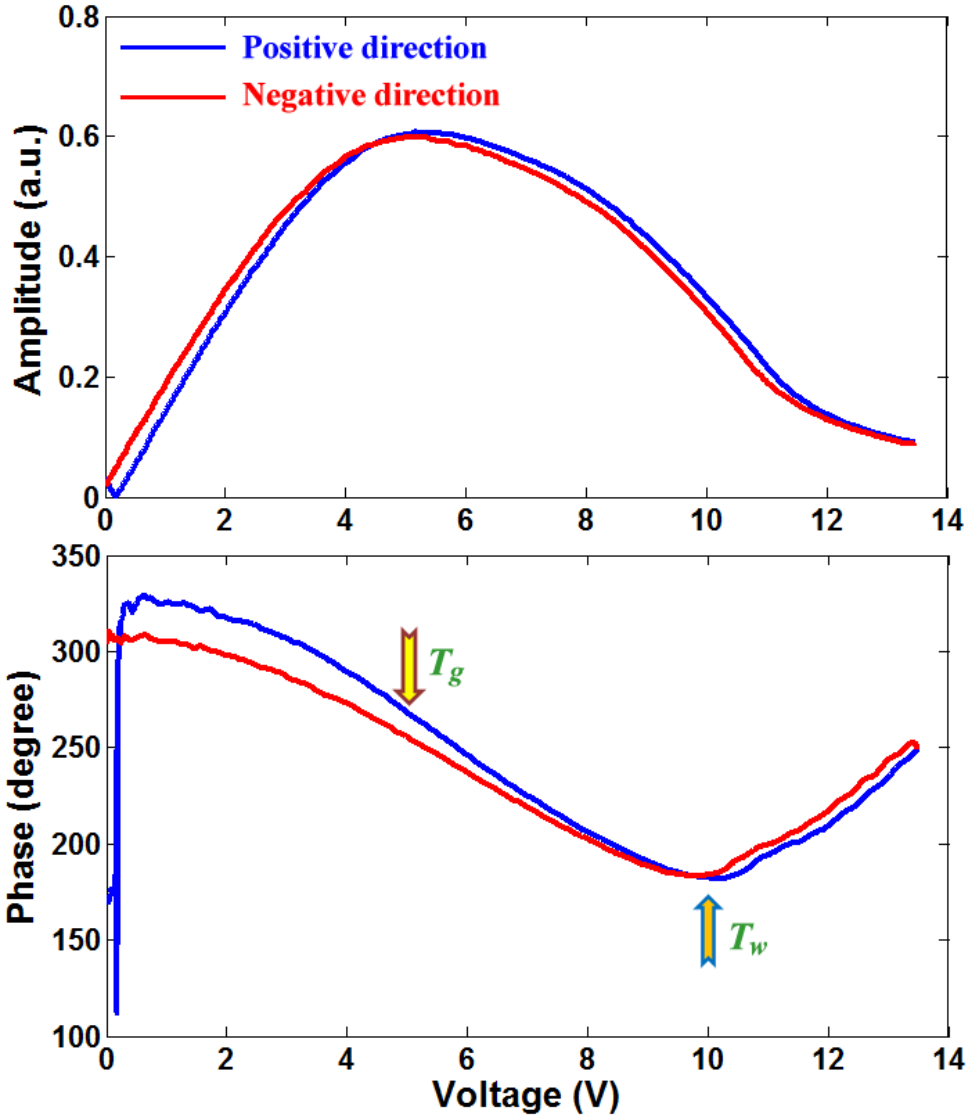

Figure 4-24 Amplitude and phase of thermomechanical oscillation driven at resonance frequency.

For Ge-As-Se-Te sample, evaporation is not observed. More interestingly, crystallization, which is a phase transition that occurs after glass transition for the chalcogenide glasses, was not observed for the thin film substrates. When the glass is in the thin film form the strong confinement increases the degree of correlation thus hindering the crystallization process [15].

4.3.4 Driving Frequency Dependence of Amplitude and Phase

In this section, frequency dependence of the amplitude and phase of the oscillations behavior is examined. Monitoring only the amplitude and phase of a thermomechanical oscillation at a specific excitation frequency can yield ample information about thermal transition events. However if a measurement is performed away from the resonant frequency range the sensitivity of the cantilever decreases and thermal events cannot be resolved. The sensitivity of the amplitude decrease as the selected driving frequency shifts away from the resonance frequency (Figure 4.25). This effect was also predicted from the theoreticalmodel, see Figure 4-26.

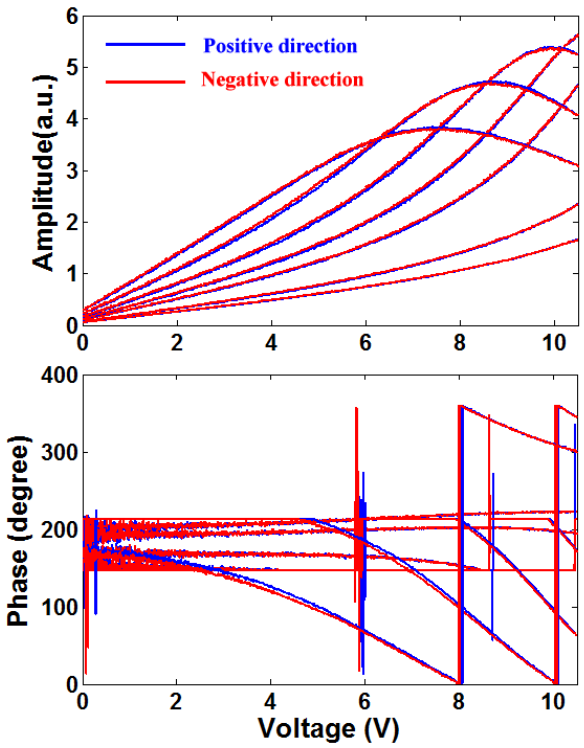

Figure 4-25 Amplitude and Phase of Thermomechanical Oscillations for different driving frequencies.

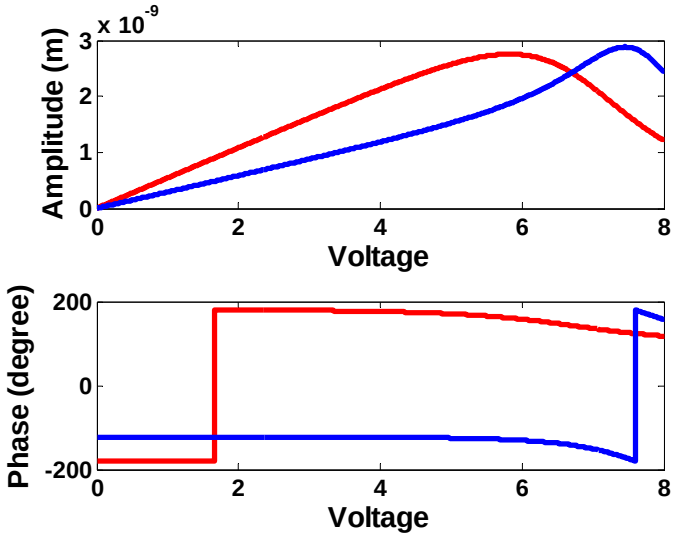

Figure 4-26 Analytical thermomechanical tesponse of amplitude and phase driven at resonance frequency and below resonance frequency.

In the above measurements the change in material properties and thermal processes are correlated. This enables identification of important thermal transition points. Time dependent characters of thermal transitions are observed. The reversible and irreversible processes can be separated. Further examination of the quantitative information about material properties requires realistic material models included in the theoretical model and extended measurements that should be performed simultaneously.

Chapter 5

Conclusion and Future Work

Firstly, thermal analysis methods were classified and discussed in detail. All these methods monitor material properties with respect to temperature difference or heat flow. It is possible to determine thermal transitions, reversible and irreversible processes, dynamical response of materials to temperature programs by using one or more of these methods. A MEMS bimetallic micro cantilever, which integrates calorimetry, thermomechanical analysis dynamical mechanical thermal analysis was fabricated, and used for thermal probing of thin film chalcogenide glasses.

The device having sample coated on it, was heated by applying a modulated voltage which induces oscillatory temperature on a linearly increasing temperature program. Simultaneously DC deflection, thermomechanical oscillation's amplitude and phase were monitored including about temperature dependencies of material properties.

To model this thermomechanical behavior of the cantilever and the sample, a mathematical model is built. By fitting the model parameters to the measurements, thermal time constant, resonance frequency, quality factor of the device were obtained. The model predicts the characteristics of the cantilever's thermomechanical behavior. From these characteristic curves thermal transition processes and their time dependency are deduced. However to obtain quantitative information, more realistic material models should be used in parallel with more data extensive measurements. The convolution of many variables affecting the thermomechanical process necessitates large number of measurements to be simultaneously performed.

Bibliography

[1] Callister, Jr. W.D., *Materials Science and Engineering An Introduction, John* Wiley & Sons, Inc., **2007**.

[2] calorimeter., Encyclopædia Britannica., **2008**., Encyclopædia Britannica Online. 7 August 2008 <http://original.britannica.com/eb/article-9018727>.

[3] Brown, E.M. (ed.), *Handbook of Thermal Analysis and Calorimetry, Volume 1 Principles and Practice*, Elsevier, **1998**.

[4] Haines, P.J. (ed.), *Principles of Thermal Analysis and Calorimetry*, Royal Society of Chemistry, **2002**.

[5] Höhne, G., Hemminger, W., Flammersheim, H.-J., *Differential Scanning Calorimetry, An Introduction for Practioners*, Springer, **1996**.

[6] Mathot, V.B.F., *Calorimetery and Thermal Analysis of Polymers*, Hanser Publishers, **1994.**

[7] Peltier effect., Encyclopædia Britannica., **2008**. Encyclopædia Britannica Online. 8 August 2008 <http://original.britannica.com/eb/article-9059021>.

[8] Olson , E. A. et al, *Scanning calorimeter for nanoliter-scale liquid samples*, APL, **2000**, Vol. 77, 17.

[9] Wunderlich, B*, Mathematical-Description of Differential Scanning Calorimetry Based on Periodic Temperature Modulation.***,** Thermochim. Acta, **1994**, Vol. 238

[10] Carpentier, L. and Descamps, M. , *Temperature-modulated differential scanning calorimetry as a specific heat spectroscopy.* J. Phys. D: Appl. Phys. 35, **2002**, Vol. 35.

BIBLIOGRAPHY

[11] Wunderlich, B., *Temperature-modulated differential scanning calorimetry of reversible and irreversible first-order transitions.,* Thermochimica Acta 330, **1999**, Vol. 330.

[12] Hourston, Douglas J. and Reading, Mike, *Modulated Temperature Differential Scanning* Calorimetry., Springer, **2006**. ISBN-10 1-4020-3749-X (HB).

[13] Collins, S., Differential Scanning Calorimetry, **2008**., *10 August 2008* <www.dur.ac.uk/n.r.cameron/Assets/Group%20talks/DSC%20presentation.ppt>

[14] Roylance, D*.,* Engineering Viscoelasticity, **2001**., *10 August 2008,* <http://ocw.mit.edu/NR/rdonlyres/Materials-Science-and-Engineering/3-11Mechanics-of-MaterialsFall1999/038732E6-CF1E-4BD0-A22E-39123ADD3337/0/visco.pdf>

[15] Gadaud, P. and Pautrot, S*, Characterization of the elasticity and anelasticity of bulk glasses by dynamical subresonant and resonant techniques***.**, Journal of Non-Crystalline Solids, **2003**, Vol. 316.

[16] Gadaud, P. and Pautrot, S. *, Application of the dynamical flexural resonance technique to industrial materials characterisation.*, Materials Science and Engineering A, **2004**, Vol. 370.

[17] Gadaud, P.**,***Temperature dependence of the mechanical behaviour of a GeAsSe glass.*, Scripta Materialia, **2001**, Vol. 45.

[18] Gadaud, P., *Characterisation of the elasticity of bulk materials and coatings by means of dynamical resonant technique.*, International Journal of Materials and Product Technology, **2006**, Vol. 26.

[19] Mitch, M. G., et al., *Phase Transition in Ultrathin Bi Films.*, Phys. Rev. Lett., **1991**, Vol. 67.

[20] Doye, J. P. K. and Calvo, F., *Entropic effects on the size dependence of cluster structure.*, Phys. Rev. Lett., 2001, Vol. 86.

BIBLIOGRAPHY

[21] Allen, L. H., et al., *Size-Dependent Melting Properties of Small Tin Particles: Nanocalorimetric Measurements.*, Phys. Rev. Lett., **1996**, Vol. 77.

[22] Buffat, Ph. and Borel, J-P., *Size effect on melting temperature of gold particles*6., Phys. Rev. A, **1976**, Vol. 13.

[23] Allen, G. L., et al., *Small particle melting of pure metals.*, Thin Solid Films, **1986**, Vol. 144.

[24] Vinci, R. P., Brown, W. L. and Hyun, S., *Thickness and temperature dependence of stress relaxation in nanoscale aluminum films.*, Appl. Phys. Lett., **2003**, Vol. 83.

[25] Verbruggen, A. H., Kalkman, A. J. and Radelaar, S., *High-temperature tensile tests and activation volume measurement of free-standing submicron Al films.*, J. Appl. Phys., **2002**, Vol. 92.

[26] Saif, M. T. A. and Haque, M. A., *Thermo-mechanical properties of nano-scale freestanding aluminum films.*, Thin Solid Films, **2005**, Vol. 484.

[27] Olson, E. A., et al, *.The design and operation of a mems differential scanning nanocalorimeter for high-speed heat capacity measurement of ultrathin films.*, J. Microelectromech. Sys., **2003**, Vol. 12.

[28] Efremov, M. Y., et al., *Glass Transition in Ultrathin Polymer Films: Calorimetric Studies*., Phys. Rev. Lett., **2003**, Vol. 91.

[29] Allen, L. H., Ober, C. K. and Braun, P. V., *Heat capacity measurements of two-dimensional self-assembled hexadecanethiol monolayers on polycrystalline gold*s., Appl. Phys. Lett., **2004**, Vol. 84.

[30] Efremov, M. Y., et al, *.Glass transition of poly(2-vinyl pyridine) and poly (methyl methacrylate): nanocalorimetry measurements.*, Thermochimica Acta, **2003**, Vol. 403.

BIBLIOGRAPHY

[31] Ramanath, G., et al., *Heat capacity measurements of Sn nanostructures using a thin-film differential scanning calorimeter with 0.2 nJ sensitivity.*, Appl. Phys. Lett., **1997**, Vol. 70.

[32] Lai, S. L., Carlsson, J. R. A. and Allen, L. H., *Melting point depression of Al clusters generated during the early stages of film growth: Nanocalorimetry measurements.*, Appl. Phys. Lett., **1998**, Vol. 72.

[33] Efremov, M. Y., et al., *Ultrasensitive, fast, thin-film differential scanning calorimeter.*, Rev. Sci. Inst., **2004**, Vol. 75.

[34] **Lai, S. L., et al.**, *High-speed (104 °C/s) scanning microcalorimetry with monolayer sensitivity (J/m2).*, Appl. Phys. Lett., **1995**, Vol. 67.

[35] McCluskey, P. J. and Vlassak, J. J., *Parallel nano-Differential Scanning Calorimetry: A New Device for Combinatorial Analysis of Complex nano-Scale Material Systems.*, Mater. Res. Soc. Symp. Proc., **1996**, Vol. 924.

[36] Welland, M. E., et al., *A femtojoule calorimeter using micromechanical sensors.*, Rev. Sci. Instrum., **1994**, Vol. 65.

[37] Gimzewski, J. K., et al., *Thermal analysis using a micromechanical calorimeter.*, Appl. Phys. Lett., **1996**, Vol. 69.

[38] Nakagawa, Y., Schafer, R. and Güntherodt, H. J., *Picojoule and submillisecond calorimetry with micromechanical probes.*, Appl. Phys. Lett., **1998**, Vol. 73.

[39] Price, D. M., et al., *Micro-thermal analysis: scanning thermal microscopy and localised thermal analysis.*, International Journal of Pharmaceutics, **1999**, Vol. 192.

[40] Price, D. M., et al., *New adventures in thermal analysis.*, Journal of Thermal Analysis and Calorimetry, **2000**, Vol. 60.

[41] Xensor Integration bv, **2008**., 15 August 2008 < http://www.xensor.nl/txtfiles/hfdfiles/prod.htm >

BIBLIOGRAPHY

[42] Senturia, Stephen S**.,** *Microsystem Design.*, Springer, **2000**.

[43] Chiao, Mu and Lin, Liwei*., Self-Buckling of Micromachined Beams Under Resistive Heating.* s.l. : Journal of Microelectromech. Systems, **2000**, Vol. 9.

[44] Lai, J., et al., *Optimization and performance of high-resolution micro-optomechanical thermal sensors.*, Sensors and Actuators A, **1997**, Vol. 58, pp. 113-119.

[45] Zhao, Yang., *Ph.D. Thesis.*, University of California, Berkeley, **2002**.

[46] Chu, H., Mehregany, M. and LMullent, R*., Analysis of tip deflection and force of a bimetallic microactuator.*, J. Micromech. Microeng., **1993**, Vol. 3.

[47] Torun, H. and Urey, H*., Thermal deflections in multilayer microstructures and athermalization.*, J. Appl. Phys., **2006**, Vol. 100.